ADVANCED BIOLOGY
www.advanced-bio.com

Chemotherapy Assessment in Advanced Multicellular 3D Models of Pancreatic Cancer: Unravelling the Importance of Spatiotemporal Mimicry of the Tumor Microenvironment

Priyanka Gupta, Camino Bermejo-Rodriguez, Hemant Kocher, Pedro A. Pérez-Mancera, and Eirini G. Velliou**

Pancreatic ductal adenocarcinoma (PDAC) is a challenge for global health with very low survival rate and high therapeutic resistance. Hence, advanced preclinical models for treatment screening are of paramount importance. Herein, chemotherapeutic (gemcitabine) assessment on novel (polyurethane) scaffold-based spatially advanced 3D multicellular PDAC models is carried out. Through comprehensive image-based analysis at the protein level, and expression analysis at the mRNA level, the importance of stromal cells is confirmed, primarily activated stellate cells in the chemoresistance of PDAC cells within the models. Furthermore, it is demonstrated that, in addition to the presence of activated stellate cells, the spatial architecture of the scaffolds, i.e., segregation/compartmentalization of the cancer and stromal zones, affect the cellular evolution and is necessary for the development of chemoresistance. These results highlight that, further to multicellularity, mapping the tumor structure/architecture and zonal complexity in 3D cancer models is important for better mimicry of the in vivo therapeutic response.

1. Introduction

Pancreatic ductal adenocarcinoma (PDAC), a cancer affecting the pancreas, is often referred to as the "silent killer," due to its asymptotic nature, which usually results in late-stage diagnosis and high mortality rate. It ranks as the fourth leading cause of cancer-related deaths worldwide.[1] The survival rate for PDAC over a span of five years is approximately 9%, a statistic that has shown minimal improvement over the past decades.[2] One of the primary reasons behind the poor outcomes associated with PDAC is its notable resistance to current treatment options, such as chemotherapy and radiotherapy.[3] The complex tumor microenvironment (TME) of PDAC plays a significant role in its progression and resistance to treatment. The TME comprises diverse cellular, biochemical, biophysical, biomechanical, and structural components that interact in intricate ways, affecting the disease evolution. For example, during the disease development, stellate cells of the pancreas get activated and they become a crucial TME element producing excessive amounts of extracellular matrix (ECM) proteins, leading to the formation of desmoplasia/fibrosis around the tumor, which is widely recognized as a significant contributor to the high treatment resistance observed in PDAC.[4–7]

PDAC research has been traditionally conducted using: i) 2D in vitro systems[8–11] or ii) in vivo animal models.[12–17] Although, 2D in vitro systems are easy to use, reproducible and have very low cost, they lack the ability to accurately mimic the in vivo tumor tissue characteristics, such as the structure and stiffness of the TME, the cellular spatial orientation, the cell–cell and cell–extracellular matrix (ECM) interactions, as well as environmental gradients.[6,18–20] In contrast, animal models provide a more realistic representation of the in vivo tissue conditions,[21–24] but come with drawbacks such as complexity, limited reproducibility, ethical issues as well as high costs.[18,24–26] Therefore, the research community is continuously exploring and developing alternative models, such as 3D cell cultures and organoids, to bridge the gap between 2D and in vivo models and to achieve an accurate representation of PDAC tissue microenvironment. Depending on the methods and the (bio-)materials used, 3D models can capture aspects of tissue topography, structure, and ECM composition.

Spheroids and hydrogels are the most common types of 3D cultures that have been used for chemotherapeutic assessment

P. Gupta, E. G. Velliou
Centre for 3D Models of Health and Disease
Division of Surgery and Interventional Science
University College London
London W1W 7TY, UK
E-mail: priyanka.g.gupta@ucl.ac.uk; e.velliou@ucl.ac.uk
C. Bermejo-Rodriguez, P. A. Pérez-Mancera
Department of Molecular and Clinical Cancer Medicine
University of Liverpool
Ashton Street, Liverpool L69 3GE, UK
H. Kocher
Centre for Tumour Biology and Experimental Cancer Medicine
Barts Cancer Institute
Queen Mary University of London
London EC1M 6BQ, UK

The ORCID identification number(s) for the author(s) of this article can be found under https://doi.org/10.1002/adbi.202300580

DOI: 10.1002/adbi.202300580

of PDAC to date,[17,27–33] while studies on polymer-based scaffolds are more limited.[34] Spheroid models are the oldest and most common 3D platform used for the development of PDAC models. They have consistently demonstrated an increased chemoresistance for multiple pancreatic cancer cell lines in comparison to 2D systems.[17,28,29]

Hydrogel-based 3D models provide structural and architectural complexity enabling more advanced mimicry of the biomechanical/biochemical tissue environment as well as longer culturing timeframes.[27,30,33,35] Similar to spheroids models, hydrogel-based 3D models of pancreatic cancer also demonstrated higher resistance to various chemotherapeutic reagents (Gemcitabine, Paclitaxel) in vitro.[30,33] Interestingly, Xie et al., compared a biomaterial free (spheroids) and hydrogel-based (alginate hydrogels) 3D cultures of BxPC-3 cells and reported that although both models showed chemoresistance on application of Gemcitabine (GEM) as compared to a 2D system, the hydrogel-based models showed higher resistance in comparison to spheroids and hence reflected better the in vivo drug efficacy. This highlighted the importance of a controlled structure and ECM composition in 3D models when conducting therapeutic assessment in vitro.[27]

Polymeric scaffold-based 3D models allow for extensive architectural and spatial tuning in combination with long-term culture (>4 weeks).[34,36–40] We have previously developed a polyurethane (PU) based polymeric scaffold PDAC model. The scaffold was generated via the thermal induced phase separation method and has high porosity (average pore size was 100–150 µm, porosity 85–90%).[40] Furthermore, we have carried out systematic chemotherapy (GEM), radiotherapy, and chemoradiotherapy assessment on this PU scaffold-based PDAC model. We observed a dose-dependent impact of both chemotherapy and radiotherapy on the viability and apoptosis of PDAC cells. We have also reported the feasibility of using the model for systematic treatment assessment both short, i.e., 24 h and long term, i.e., 17 d. Such time-frame enables long-term observations of the evolution of PDAC post-treatment as well as the possibility of fractionated treatment in vitro.[34]

The above studies present substantial progress towards better mimicry of the TME in vitro. However, as previously mentioned, the in vivo PDAC tumor niche is not monocellular; rather it is a complex, dynamic, inter-dependent niche of various cell types, e.g., cancer cells, stellate cells, cancer associated fibroblasts (CAFs), endothelial cells, immune cells, all contributing into the disease progression and treatment resistance.[3,41–45] Therefore, studies on the development and treatment screening on multicellular 3D models of PDAC have recently emerged.[31,46–55] Most multicellular PDAC 3D models are either spheroids or hydrogel-based systems containing pancreatic cancer cells and fibroblastic cells (CAFs or activated pancreatic stellate cells). For example, Ware et al. observed a reduced GEM diffusion in PDAC spheroids of various pancreatic cancer cell lines (PANC-1, AsPC-1, BxPC-3, Capan-1 and MIA PaCa-2) in the presence of primary stellate cells as compared to monocellular cancer cell spheroids.[55] Similarly, Broekgaarden et al. reported increased resistance to oxaliplatin within multicellular spheroid models of patient derived CAFs and pancreatic cancer cell lines (MIA PaCa-2 and AsPC-1).[51]

Osuna de la Peña et al. designed biomimetic peptide amphiphile (PA-ECM) hydrogels containing collagen I (COL I), fibronectin (FN), laminin (LAM) and hyaluronan and cultured within them patient derived PDAC cells, stellate cells and macrophages for up to 14 d.[52] A comparison of the cell evolution post-treatment with GEM, triptolide and their combination, took place between simple spheroids, Matrigel assisted organoids and 2D cultures. Only the PA-ECM cultures were able to consistently reproduce the in vivo patient derived xenograft (PDX) response, while spheroids and 2D monolayers showed the opposite response pattern. In addition, the PA-ECM models were able to support the stromal cells better than the other models, collectively suggesting the importance of structural, biochemical and cellular control in 3D models. Similar observations supporting the importance of stromal cells in chemoresistance within hydrogels were also reported by Curvello et al.[53] Monteiro et al. developed a novel, tunable, compartmentalized "cancer on a bead" model of PDAC using PANC-1 cancer cells and CAFs on Gelatin methacrylate (GelMA) and hyaluronic acid (HA) beads and compared it to simple monocellular and multicellular spheroids.[50] The "cancer on a bead" model showed 1.8- and 1.16-times higher resistance to GEM when compared to the monocellular and multicellular spheroids, respectively. These data further highlight the importance of mimicking the spatial architecture/separation of the cancer and stromal compartments within an in vitro 3D model. We have previously developed a novel, multicellular, hybrid, polyurethane scaffold-based model. The model consisted of a FN coated PU cylinder/core where pancreatic cancer cells were seeded (PANC-1 cells) surrounded by an external COL I-coated cuboid where activated stellate cells (PS-1) and endothelial cell (HMECs) were seeded. We have shown the feasibility of long-term culture (up to 5 weeks) in this complex zonal model, which recapitulates the desmoplastic/fibrotic reaction of PDAC.[37]

In our current work, we investigate the importance of multicellularity as well as spatiotemporal cellular and matrix modeling on the evolution and treatment response of PDAC in 3D PU highly porous scaffolds (**Figure 1**). More specifically, we performed a systematic comparative study of the PDAC cellular evolution and chemotherapy (GEM) response in: i) a single ECM coated PU monocellular (cancer cells only) scaffold model, ii) a single ECM coated PU multicellular (triculture) scaffold model, iii) a PU zonal/dual monocellular (cancer cells only) scaffold model consisting of a central cancer mass, surrounded by an external cell-free, ECM (COL I) periphery and iv) our novel zonal/dual multicellular (tri-culture) PU scaffold model.[37] To the best of our knowledge there is no such study to date and our findings highlight the importance of spatiotemporal design of cellular and matrix components in 3D cancer models.

2. Experimental Section

2.1. Polymer Scaffold Preparation and Surface Modification

Poly urethane (PU) scaffolds were fabricated via the thermal induced phase separation (TIPS) method as reported previously.[34,39,40,56] The scaffolds were then cut at appropriate sizes (see Sections 2.3.1 and 2.3.2) and sterilized by exposing them to 70% ethanol (3 h) and UV ray (1 h). Thereafter, the generated scaffolds were surface modified with fibronectin (FN) and/or collagen I (COL I) depending on the scaffold configuration, for

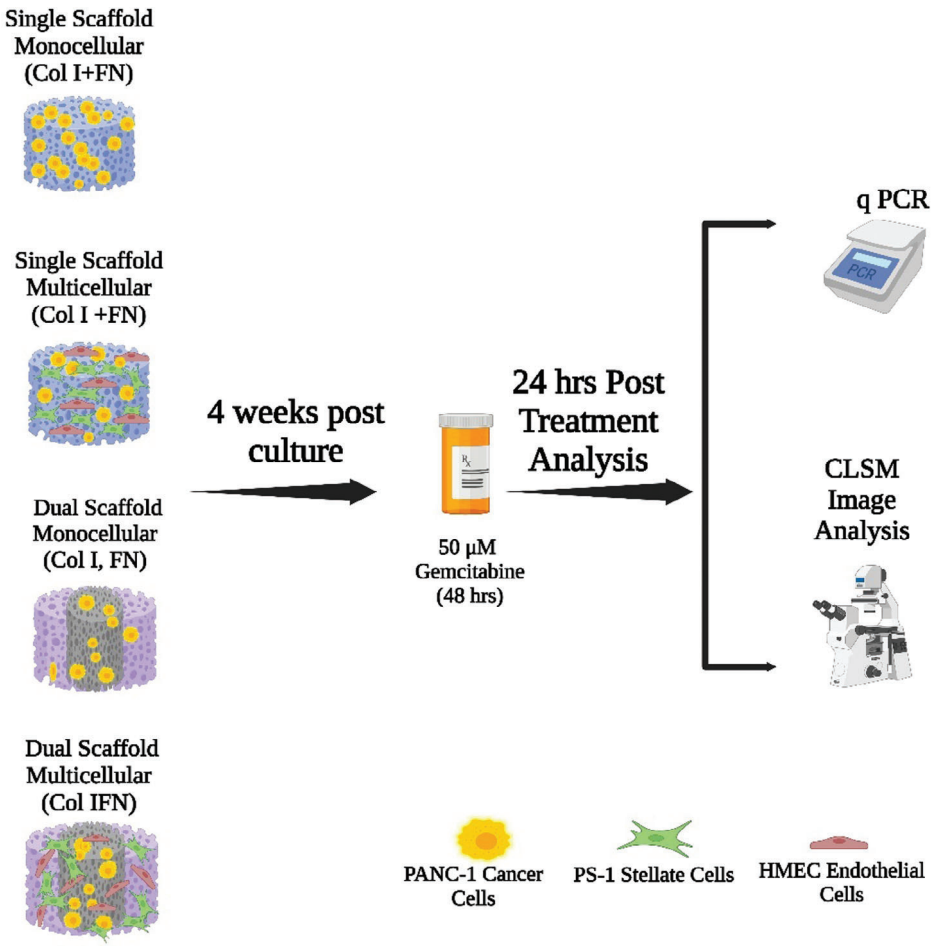

Figure 1. Schematic representation for the experimental outline of the chemotherapeutic assessment (GEM) on polyurethane (PU) scaffold based multicellular models of PDAC (Created with BioRender.com).

ECM mimicry[37] (Figure 1). More specifically, it was previously shown that stromal cells, i.e., endothelial and stellate cells show a preference to COL I for optimal growth and spatial density in the scaffolds while PDAC cells show a preference to FN. Therefore, for the multicellular zonal scaffold configuration, the cancer polymeric scaffold (PU) core was FN coated and surrounded by a COL I external PU scaffold ring, where the stroma cells were seeded (dual scaffold multicellular, Figure 1). To assess the impact of the presence of the stroma cells on the cancer growth and treatment response, a comparative analysis with scaffolds was run composed by a cell free COL I coated external PU ring, and cancer cells in the FN coated center PU core (dual scaffold monocellular, Figure 1). To assess the importance of spatial segregation of different types of the tumor microenvironment in the scaffolds, a comparative study with single scaffolds (coated with both COL I and FN on a 1:1 ratio to ensure optimal growth of all cell types) was also run. More specifically, multicellular single scaffolds consisting of cancer and stroma (stellate and endothelial) cells (single scaffold multicellular, Figure 1) were developed. Monocellular single scaffolds were also developed, consisting of cancer cells only (single scaffold monocellular, Figure 1), coated with COL I and FN on a 1:1 ratio.

2.2. 2D Cell Culture

The human pancreatic adenocarcinoma cell line *PANC-1* (ATCC, UK) was expanded in Dulbecco's modified Eagle's medium (DMEM) with high glucose (SIGMA-Aldrich, Merck, UK) supplemented with 10% fetal bovine serum (FBS, Fisher Scientific, UK), 1% penicillin/streptomycin (Fisher Scientific, UK) and 2×10^{-3} M L-glutamine (Sigma-Aldrich, Merck, UK) in a humidified incubator at 37 °C with 5% CO_2.

The human microvascular endothelial cell (HMEC) line CRL-3243 (ATCC, UK) was expanded in MCDB 131 medium (GIBCO, Thermo Fisher, UK) supplemented with 10% FBS, 1% penicillin/streptomycin, 2×10^{-3} M L-glutamine, 10 ng mL^{-1} epidermal growth factor (SIGMA- Aldrich, Merck, UK) and 1 µg mL^{-1} hydrocortisone (SIGMA- Aldrich, Merck, UK) in a humidified incubator at 37 °C with 5% CO_2.

The immortalized human pancreatic stellate cell line PS-1[57,58] was expanded in DMEM (SIGMA-Aldrich, Merck, UK) supplemented with 10% fetal bovine serum (FBS, Fisher Scientific, UK), 1% penicillin/streptomycin (Fisher Scientific, UK) and 2×10^{-3} M L-glutamine (Sigma-Aldrich, Merck, UK) in a humidified incubator at 37 °C with 5% CO_2.

All cells were passaged regularly on reaching 80–90% confluency with TrypLE (GIBCO, Thermo Fisher, UK) till the required cell densities were obtained.

2.3. 3D Models

2.3.1. Single Scaffold Based 3D Models

For the development of the single scaffold models (multicellular and monocellular—see also Section 2.1), PU scaffolds ($5 \times 5 \times 5$ mm^3) coated with both collagen I (COL I) and fibronectin (FN) (1:1 ratio) were seeded with 0.5×10^6 cells/scaffold/cell type as previously described.[34,39,40] More specifically, for the multicellular models PANC-1, PS-1 and HMEC cells were seeded while for the monocellular cancer model (control) PANC-1 cells were seeded. Thereafter, the scaffolds were placed in 24-well plates and cultured for 28 d (4 weeks) in a humidified incubator at 37 °C with 5% CO_2.

2.3.2. Dual Scaffold Based (Zonal) 3D Models

For the development of the dual (zonal) scaffold based models (multicellular and monocellular—see also section 2.1) we used as a basis our previously developed zonal PDAC model, which we have shown that recapitulates the spatial architecture of the PDAC tumour microenvironment.[37,59] More specifically, two separate PU zones (a hollow cuboid/external ring with dimensions of $7 \times 7 \times 5$ mm^3 and a solid inner cylinder/core of diameter 3 mm and height of 5 mm) were fabricated. The outer cuboid/external ring was coated with COL I while the inner cylinder was coated with FN.

For the development of the multicellular dual scaffold model (Figure 1), 0.25×10^6 PANC-1 cancer cells were seeded on to the inner cancer compartment (resuspended in 10 µL of media) and cultured for 7 d. This cell number was selected to ensure the same cell spatial density as the single scaffold configuration. After 7 d, PS-1 stellate cells and HMEC cells were added to the outer stromal compartment at a seeding density of 0.5×10^6 cells/cell type and then plugged together with the inner cylinder to assemble the complete hybrid zonal model. Thereafter, the triculture was monitored for an additional 21 d (total 4 weeks). The difference in seeding times between the cancer core and the stroma external ring was decided, to ensure optimal growth of cell types by week 4 of culture as well as to avoid in vitro ageing of the stroma.[37] The cell ratio was PANC-1:PS-1: HMEC = 1:2:2 at the time of seeding.[37] For the development of the monocellular dual scaffold model (control) a dual scaffold with an inner compartment (FN coated) seeded with PANC-1 cells surrounded by an acellular (cell free) outer stromal compartment (COL I coated) was fabricated and monitored for 4 weeks.

2.4. Treatment Protocol in 3D scaffolds

At week 4 of culture, all models were exposed to chemotherapy with 50×10^{-6} M of Gemcitabine (GEM), a well-known DNA binding drug. The drug concentration was chosen based on the previous comparative assessment wherein it was observed that 50×10^{-6} M GEM was nearest to the drug's IC_{50} within our 3D PU PDAC model.[34] GEM was added to the culture for 1 feeding cycle/media change (48 h) and removed thereafter.[34] The scaffolds were characterized 24 h post-treatment (24 h after the removal of GEM) with sectioning, staining, advanced imaging and qPCR analysis.

2.5. Spatial Evaluation of Live and Dead Cells in the Scaffolds

To visualize the spatial distribution of live and dead cells post-treatment, scaffolds were collected (see also Section 2.4), snap frozen in liquid nitrogen for 15 min and then preserved at −80 °C.[34,37,39,40] For live/dead cell analysis, Live/Dead Viability/Cytotoxicity kit was used (Molecular Probes, Thermo Scientific, UK). Prior to analysis scaffolds were sectioned, stained with 2×10^{-6} M of calcein-AM (4×10^{-3} M stock) and 4×10^{-6} M of ethidium homodimer (2×10^{-3} M stock) and incubated at 37 °C for 1 h. The solution was then removed, and samples were washed twice in PBS followed by imaging using a Zeiss 880 inverted confocal microscope (Zeiss, UK) or Nikon inverted confocal microscope (Nikon, UK).

2.6. Spatial Evaluation of Apoptotic Cells (Caspase 3/7) in the Scaffolds

The caspase 3/7 activity was visualized and quantified in situ to assess the induction of cellular apoptosis. Scaffolds were collected and processed as described above (Section 2.5). Thereafter, the scaffolds were incubated in culture medium containing i) the Cell Event Caspase-3/7 green detection reagent (Fisher Scientific, UK) and (ii) DAPI (Fisher Scientific, UK) for 1 hour at 37 °C. The presence of caspase 3/7 positive cells (green) was immediately evaluated with a Zeiss 880 inverted confocal microscope (Zeiss UK) or Nikon inverted confocal microscope (Nikon, UK).

2.7. Immunofluorescence Assay

In situ immunofluorescence (IF) staining of the scaffolds was carried out for spatial determination of (i) the different cell types with von Willebrand factor (vWFR, HMEC), αSMA (PS-1), and pan-Cytokeratin (PANC-1) and (ii) ECM production (Collagen I). As per Sections 2.5 and 2.6, scaffolds were snap frozen at specific time points and further processed. More specifically, scaffolds were sectioned and fixed for 2–4 h in 4% w/v paraformaldehyde (SIGMA- Aldrich, Merck, UK). Sections were then permeabilized for 2 h with 0.1% Triton -X solution (SIGMA-Aldrich, Merck, UK). This was followed by a series of sequential blocking with either 10% donkey serum or 10% rabbit serum solution, overnight staining with primary antibodies (Table S1, Supporting Information) and secondary antibodies was carried out. All samples were costained with DAPI. Each step employed a solvent containing 1% w/v bovine serum albumin (Sigma-Aldrich, Merck, UK) and 0.5% v/v Tween-20 (Promega, UK).

2.8. Confocal Laser Scanning Microscopy (CLSM) Imaging

Immunofluorescent samples were imaged with a Zeiss 880 inverted confocal microscope (Zeiss, UK) and processed with the Zen Black software using the following lasers and filters: i) 405 nm (for DAPI), ii) 488 nm (for Alexa Fluor 488, Dylight 488), iii) 561 nm (for Alexa Fluor 555, Dylight 550) and iv) 643 nm (for Alexa Fluor 647, Dylight 650) for 2 sequential scans. Confocal images were captured using a 10× dry objective, with a 512 × 512-pixel resolution and 15–25 µm Z-stack distance, as previously described.[34,37,40] Multiple scaffolds and multiple sections per scaffold were imaged to ensure reproducibility. Representative images are presented in this original article.

2.9. Image Analysis

For the quantitative evaluation of i) live (green) and dead (red) population and ii) the caspase positive/apoptotic (green) and non-apoptotic (blue) population of each image, the percentage of green versus red (live/dead) or green versus blue (caspase positive /caspase negative) areas of each image were calculated using Image J software (Wayne Rasband, NIH, Bethesda, MD, USA) as previously described.[34,37,39,40] The particle analyzer macro (Image J, Wayne Rasband, NIH, Bethesda, MD, USA) was used in each individual channel (green or read for live/dead and green or blue for the caspase 3/7 respectively).

For the quantitative evaluation of Collagen I intensity, the mean gray value of COL I was measured using the particle Analyzer macro (Image J, Wayne Rasband, NIH, Bethesda, MD, USA), which was used only on the channel of interest.

As described above, multiple scaffold sections (at least 3) from at least 3 replicate scaffolds were analyzed for each condition to ensure reproducibility of the results.

2.10. mRNA Extraction, cDNA Synthesis and qPCR (Quantitative Polymerase Chain Reaction) Analysis

Total RNA from all the 3D models under study (both before treatment, i.e., at week 4 of culture, and 24 h post-treatment) was extracted using the RNeasy mini kit (Qiagen, UK) as per manufacturer's instructions and stored at −80 °C. The total RNA obtained was quantified and assessed for integrity using the NanoDrop. cDNA synthesis was carried out using RevertAid H Minus 1st strand cDNA synthesis kit (Thermo Scientifics, UK) on the T100 Thermal Cycler (Bio-Rad, Watford, UK). cDNA was stored at −20 °C. Minimum information for publication of quantitative real-time PCR experiments (MIQE) guidelines was followed during designing of primer pairs[60] (Table S2, Supporting Information). The annealing temperature was set to 60 °C and the primer pairs were obtained from Eurofins Genomics (Ebersberg, Germany). iTaq Universal SYBR Green Supermix was used to amplify the target gene in 10 µL reactions composed of 20 ng sample and 0.2 × 10^{-6} M primer concentration. The reaction ran for 40 cycles on the CFX96 Touch System (both from Bio-Rad, Watford, UK). Each sample was tested in triplicates. The ΔCT and $2^{-\Delta CT}$ method[61] were used to analyze the relative gene expression normalized to the reference gene glyceraldehyde 3-phosphate dehydrogenase (GAPDH).The following markers were assessed at selected time points for all scaffold configurations under study (Figure 1): i) Epithelial marker E-Cadherin (CDH1), ii) mesenchymal marker N-Cadherin (CDH2), iii) COL I, iv) matrix metalloproteinases (MMP2 and MMP9), v) hypoxia inducible factor 1-alpha (HIF 1-α) and vi) vascular endothelial growth factor A (VEGF-A)

2.11. Statistical Analysis

Statistical analysis was performed for at least three independent experiments with at least three replicates per time-point ($N \geq 3$, $n \geq 3$). Analysis of variance (two-way ANOVA) followed by the Bonferroni's multiple comparison test using the Graph Pad Prism software (version 9.4 for Windows) was carried out to find statistically significant differences between data ($p < 0.05$). Untreated samples were considered as control in all cases. The error bars in the graphs represent standard error of mean.

3. Results

As described in Sections 2.1, 2.3, and 2.4, to assess the impact of multicellularity and cell compartmentalization in the 3D PDAC scaffolds, on cellular behavior, characteristics as well as on the response to chemotherapy, 50 × 10^{-6} M of the chemotherapeutic reagent GEM was administered to all 3D scaffold configurations, i.e., single and dual multicellular as well as single and dual monocellular scaffolds, after 4 weeks in culture for one feeding/media change cycle, i.e., 48 h (see also Figure 1). Thereafter, 24 h post-treatment, both treated and untreated scaffolds were analyzed for viability and apoptosis (Section 3.1), for distribution of the various cell types (Section 3.2), for COL I presence (Section 3.3) and for mRNA expression of markers related to cellular phenotype (epithelial, mesenchymal), ECM presence and remodeling (COL I, MMP2, MMP9), hypoxia (HIF 1-α) and VEGF-A (Section 3.4).

3.1. Assessment of Postchemotherapy Cellular Viability and Apoptosis within Single and Dual Scaffolds

Viability and apoptosis postchemotherapy treatment were assessed via scaffold sectioning, in situ staining and CLSM imaging. For the dual scaffold monocellular and multicellular models, prior to imaging, the inner compartment (cancer cells) was separated from outer compartment (stellate and endothelial cells), enabling a more accurate observation of the effect of GEM on the different compartments (cancer and stroma). Quantification of cell viability and apoptosis in single PDAC scaffolds are shown in **Figures 2** and **3**, respectively. The increased complexity in viability and apoptosis response to chemotherapy in dual PDAC scaffolds is displayed in **Figures 4** and **5**, respectively.

As observed in Figure 2, both monocellular and multicellular single scaffold models, showed significant and similar reduction in cellular viability post-GEM treatment, indicating that the presence of the stromal cells did not affect the overall cell viability, at least in these scaffold configurations. Furthermore, a significantly upregulated expression of Caspase 3/7 was observed post-GEM treatment for both single monocellular and multicellular scaffolds (Figure 3), further supporting the effectiveness of the drug in these models, irrespective of the cellular composition.

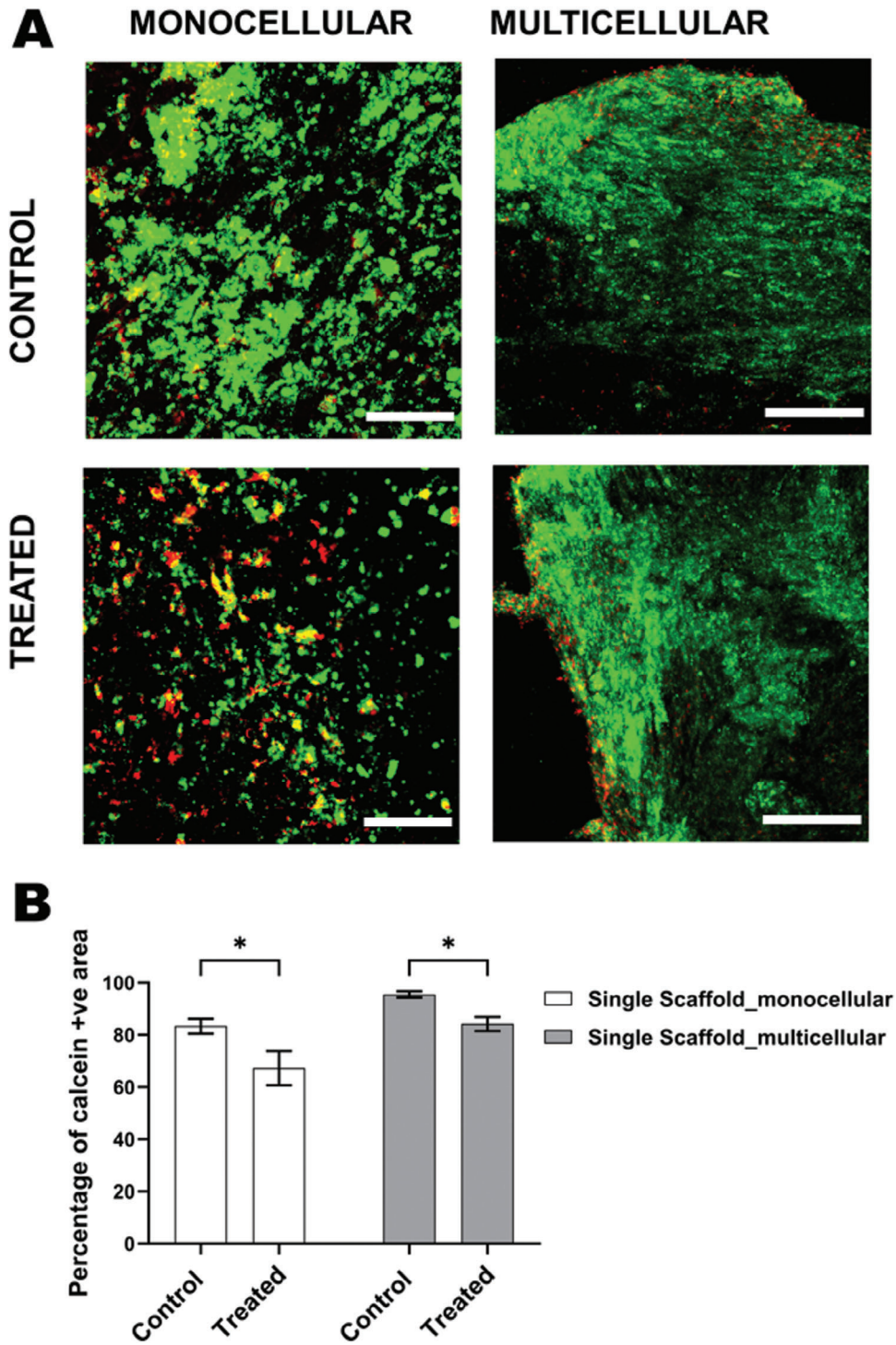

Figure 2. Effect of the chemotherapeutic agent GEM within single scaffold monocellular and single scaffold multicellular models, 24 h post-treatment. A) Representative images of sections of the scaffolds following live-dead staining. Green and red areas signify live cell and dead cell populations respectively. B) Image based analysis-quantification of live (green) image areas. Scale bar = 200 μm.

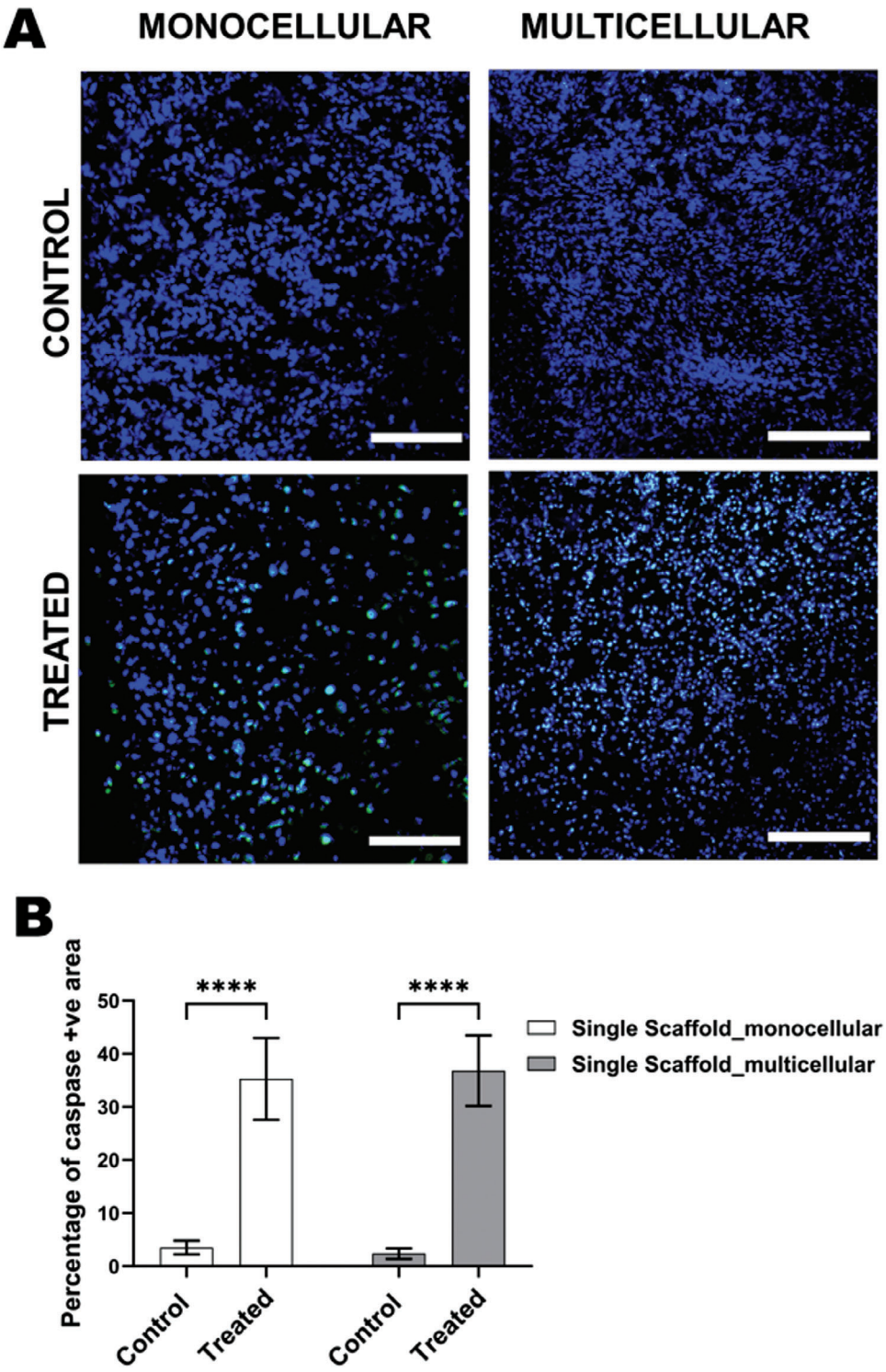

Figure 3. Effect of the chemotherapeutic agent GEM within single scaffold monocellular and single scaffold multicellular models 24 h post- treatment. A) Representative images of sections of the scaffolds for apoptosis (caspase 3/7 (green) staining). Nuclei are stained with DAPI (blue). B) Image based analysis-quantification of apoptotic (green) image areas. Scale bar = 200 μm.

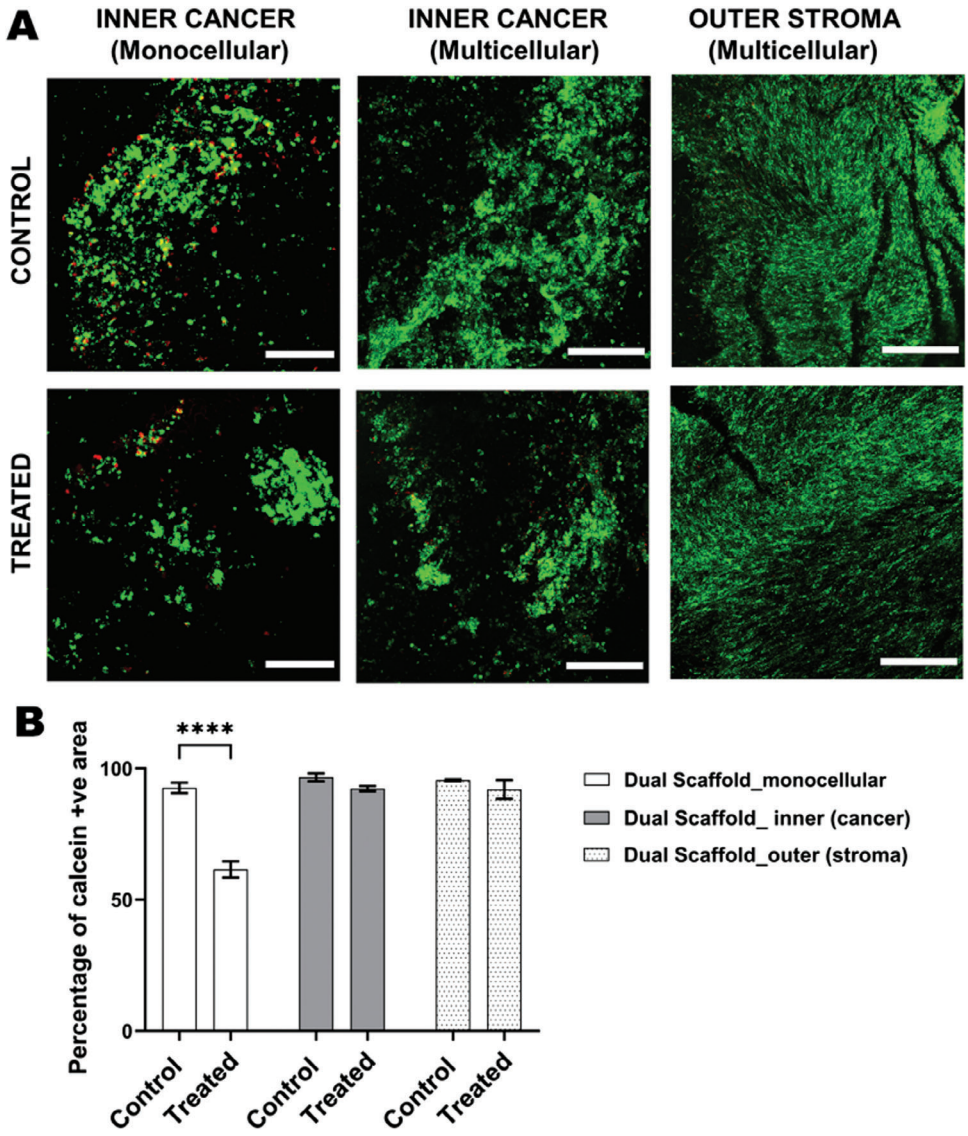

Figure 4. Effect of the chemotherapeutic agent GEM within the dual scaffold monocellular and dual scaffold multicellular models, 24 h post-treatment. A) Representative images of sections of the scaffolds following live-dead staining. Green and red areas signify live cell and dead cell populations respectively. B) Image analysis-based quantification of live (green) image areas. Scale bar = 200 μm.

Interestingly, the analysis of the dual scaffold models showed that stromal cells enhanced resistance to GEM. While monocultures exhibited a significant decrease in cellular viability in response to GEM, the presence of stroma cells drastically enhanced cell viability both in the inner and the outer compartments (Figure 4). With respect to apoptosis, a significant increase in Caspase 3/7 positive cells was observed post GEM treatment on both monocellular and multicellular dual scaffolds (Figure 5). However much higher apoptosis level was observed in the monocellular dual scaffold as compared to the multicellular scaffold (Figure 5). For the dual multicellular scaffold, when comparing the inner (cancer) with the outer (stroma: stellate and endothelial) compartments, higher apoptosis was observed in the latter.

Collectively, our data indicate that the presence of the stromal cells in a separate scaffold compartment plays a role in maintaining cellular viability and decreasing apoptosis specifically for the cancer cells, post-treatment with GEM. This is an indication that the dual scaffold multicellular model can promote GEM resistance of pancreatic cancer cells.

3.2. Assessment of Cellular Distribution within Single and Dual Multicellular Scaffolds

As described in Sections 2.7 and 2.8, IF staining and CLSM imaging was carried out to assess the cellular distribution, as well as the impact of GEM on different cell types, i.e., cancer cells, stellate cells and endothelial cells for all scaffold configurations under study.

Generally, we observed a heterogenous cell distribution within the single scaffold multicellular model, for both treated and

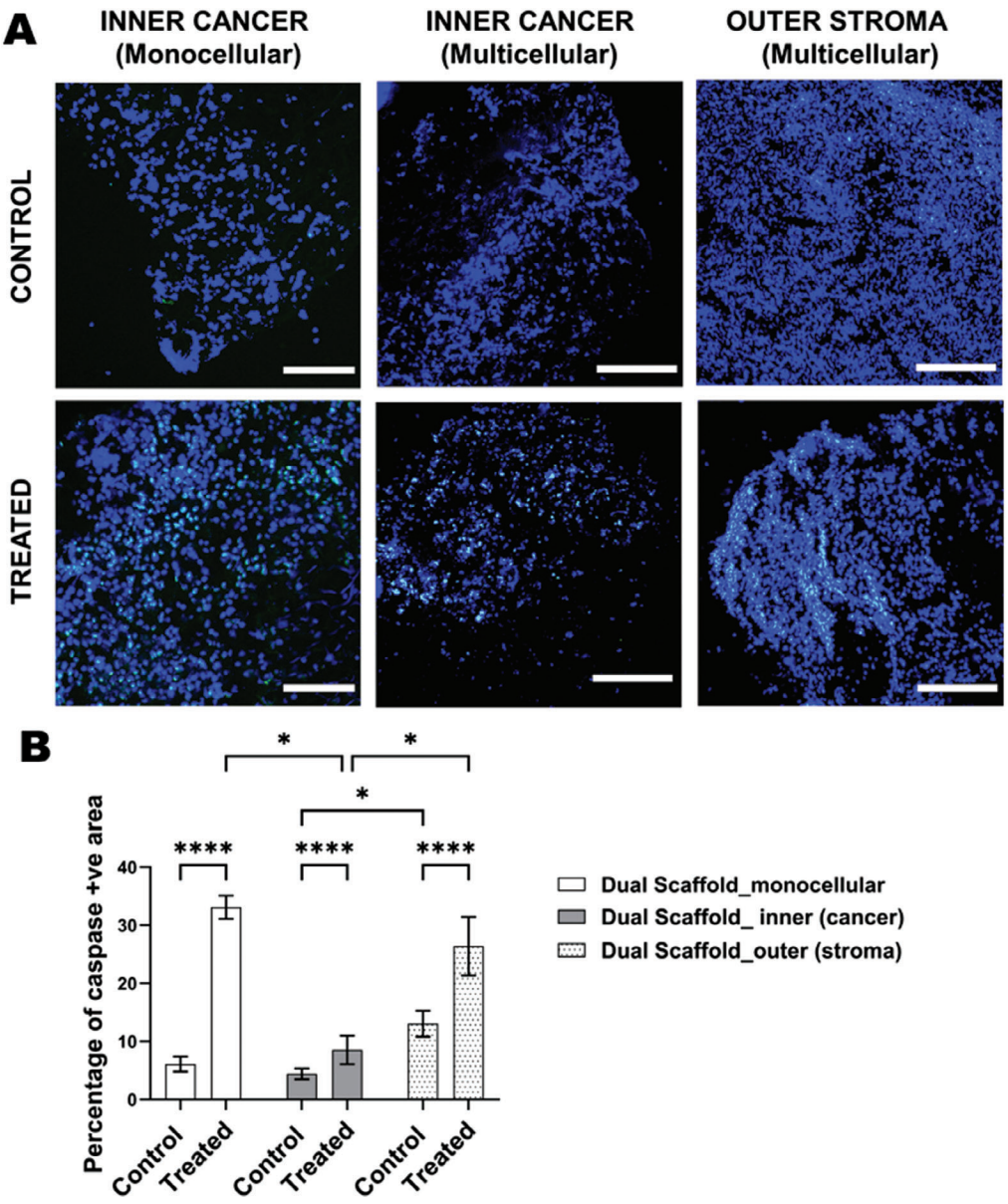

Figure 5. Effect of the chemotherapeutic agent GEM within the dual scaffold monocellular and dual scaffold multicellular models. A) Representative images of sections of the scaffolds for apoptosis (caspase 3/7 (green) staining). Nuclei are stained with DAPI (blue). B) Image based analysis-quantification of apoptotic (green) image areas. Scale bar = 200 μm.

untreated scaffolds. More specifically, we detected areas of the single scaffold richer in stellate cells wherein they formed their own niche (**Figure** 6A,B,D,E), as well as areas which were less populated with stellate cells (Figure 6C,F). In areas rich/dense with stellate cells we observed less growth of cancer cells and lowered presence of endothelial cells, while in areas less dense with stellate cells we observed a substantial growth of endothelial cells along with the cancer cells, forming a cancer-endothelial cell niche (Figure 6C). Interestingly, in post-GEM treatment cultures, an increased number of endothelial cells was observed within the single scaffold model. This can be attributed to the decrease in the number of stellate cells post-treatment, allowing the endothelial cells to proliferate within 24 h after removal of the drug (Figure 6D,E).

Within the dual scaffold multicellular model (**Figure** 7), the inner cancer compartment showed a mixed population of cancer cells (pan-cytokeratin positive and negative). We also detected endothelial cells within the inner compartment localized with the cancer cells (Figure 7A,B,E,F), a similar pattern to the one observed in the single scaffold model. This observation is of particular interest as it highlights the model's ability to support and replicate cellular migration from the outer stromal compartment to the inner cancer compartment. The outer stromal compartment primarily consisted of dense pancreatic

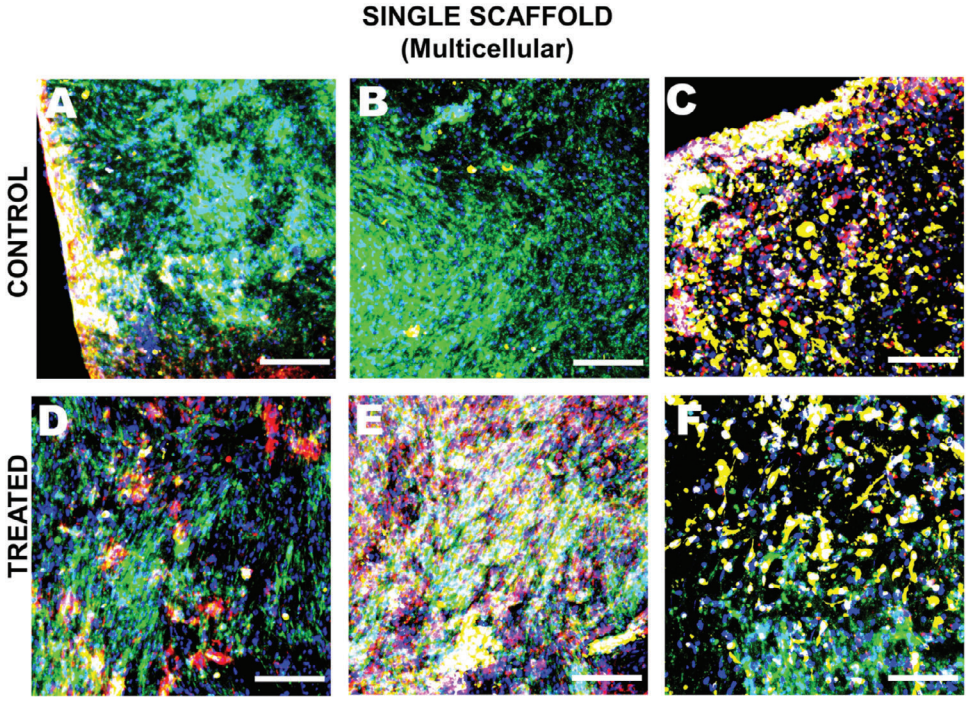

Figure 6. Representative immunofluorescence images of sections of the single multicellular scaffolds showing cellular distribution A–C) pre- and D–F) post-GEM treatment. PANC-1 PDAC cells are imaged in yellow (pan-Cytokeratin), PS-1 stellate cells are in green (αSMA), and HMEC endothelial cells are in red (vWFR). All cells were counter-stained with DAPI (blue). Scale bar = 200 μm.

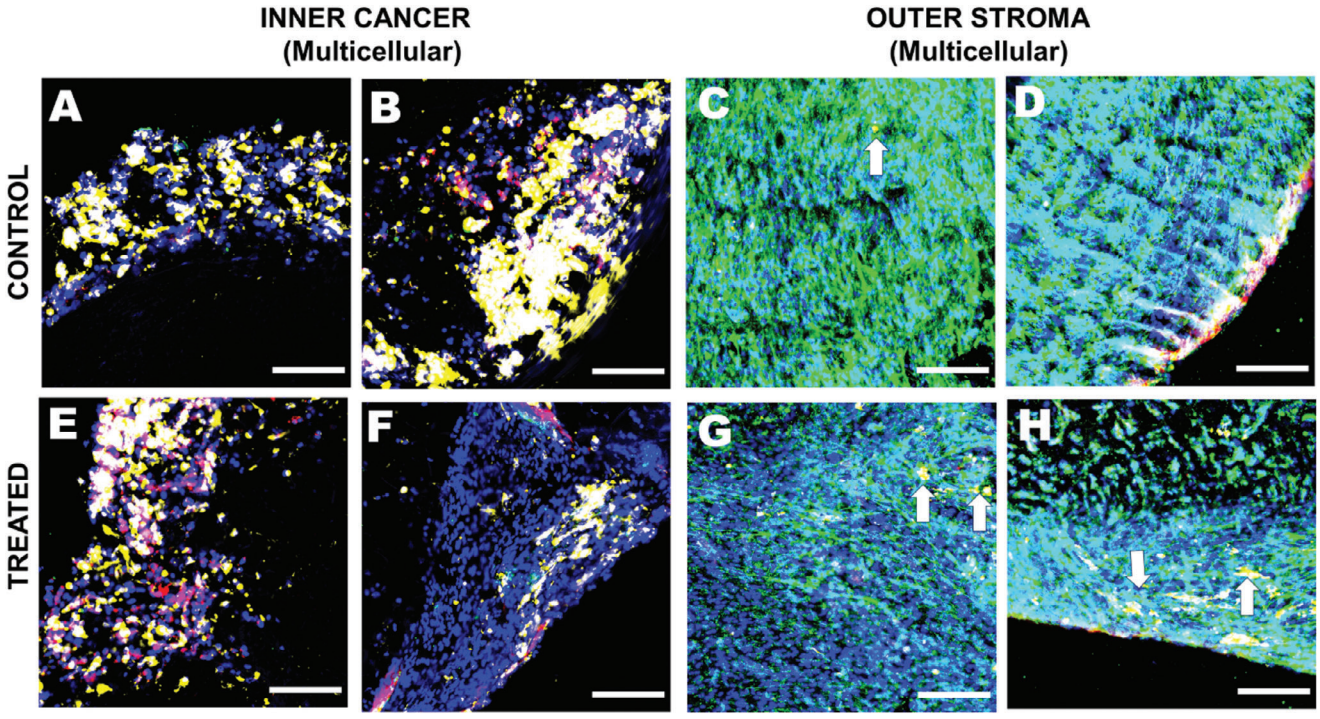

Figure 7. Representative immunofluorescence images of sections of the dual multicellular scaffolds showing the cellular distribution A–D) pre- and E-H) post-GEM treatment. A,B, E,F: inner cancer compartment; C,D, G,H: outer stroma compartment. PANC-1 PDAC cells are imaged in yellow (pan-cytokeratin staining), PS-1 stellate cells are in green (αSMA staining), and HMEC endothelial cells are in red (vWFR staining). White arrows indicate PANC-1 cancer cells within the stroma. All cells were counter-stained with DAPI (blue). Scale bar = 200 μm.

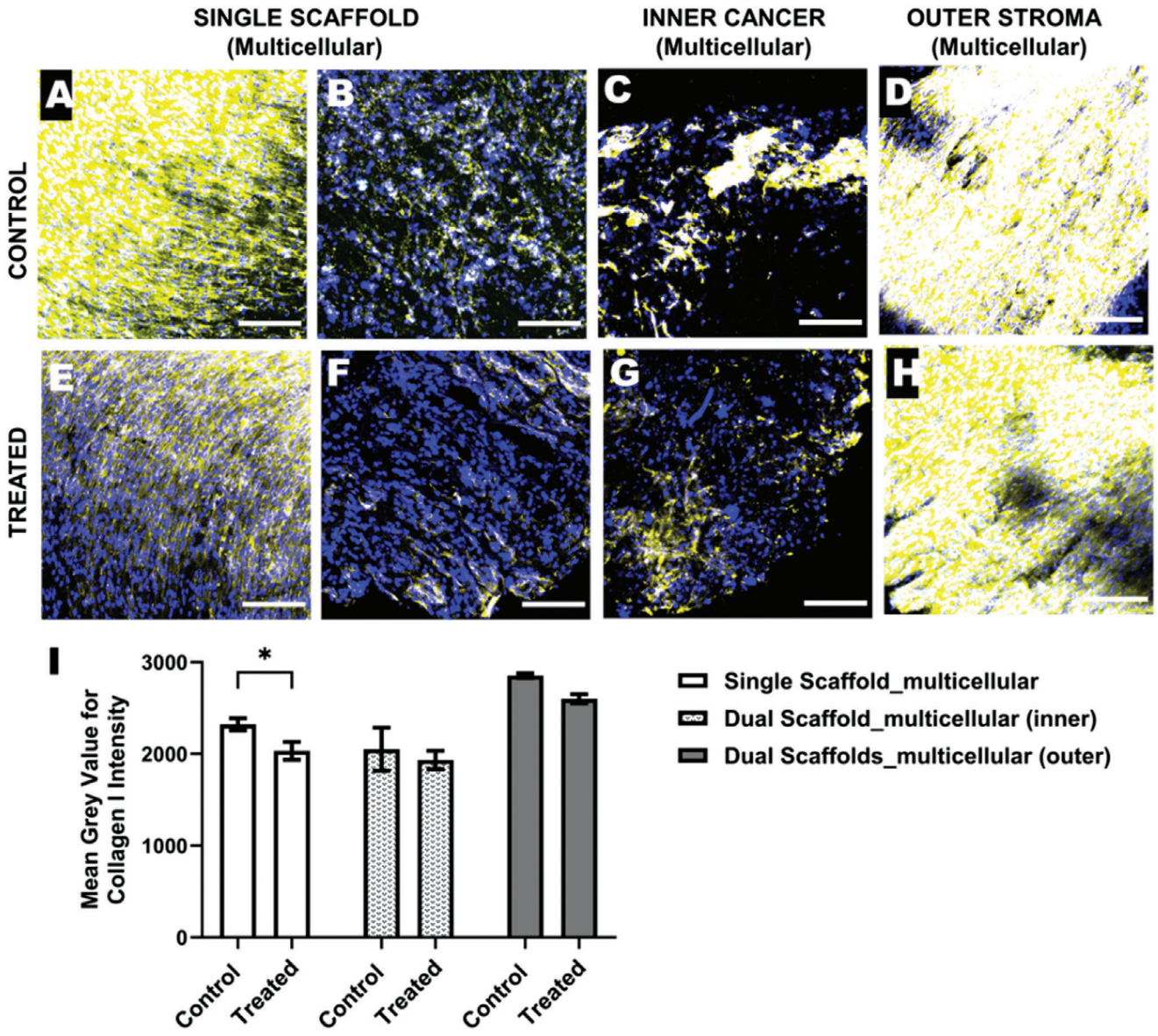

Figure 8. Representative immunofluorescence of sections of the single and dual multicellular scaffolds showing the distribution of Collagen I (COL I) pre- and post-24 h from GEM treatment. A,B) Single Scaffold Control; C,D) Dual scaffold Control; EF) Single scaffold GEM treated; G,H) Dual scaffold GEM treated. Cell nuclei were stained with DAPI (blue). I: Image based analysis-quantification of COL I positive (yellow) image areas. Scale bar = 200 μm.

stellate cells, with the endothelial cells mainly found to grow more at the periphery/edge of the scaffolds (Figure 7C,D). We also observed some degree of phenotypic changes (loss of spindle structure) for the stellate cells post-treatment with GEM (Figure 7G,H).

3.3. Assessment of Collagen I ECM Protein Presence within Single and Dual Scaffolds

We have previously reported that PS-1 stellate cells in our dual scaffold multicellular model showed the presence of excessive amount of COL I. Herein, we have verified the effect of GEM on the COL I protein presence within the single and dual multicellular scaffolds. **Figure 8** shows representative images of immunofluorescence staining for human specific COL I for both single and dual multicellular scaffold models.

Prior to GEM treatment, we observed the presence of substantial amounts of COL I both in the single scaffold model and the stromal compartment of the dual scaffold model, deposited primarily by the stellate cells (Figure 8A,D). Similarly, to the pattern of the cell distribution in the single scaffold (Figure 6), we observe heterogeneity in COL I secretion in the single scaffold, depending on the stellate cell density (Figure 8A,B), while we observe consistently excessive amounts of COL I secretion in the outer compartment of the dual multicellular scaffold (Figure 8D,I). PANC-1 cancer cells within the dual scaffold model also showed some amount of COL I secretion as we have previously reported

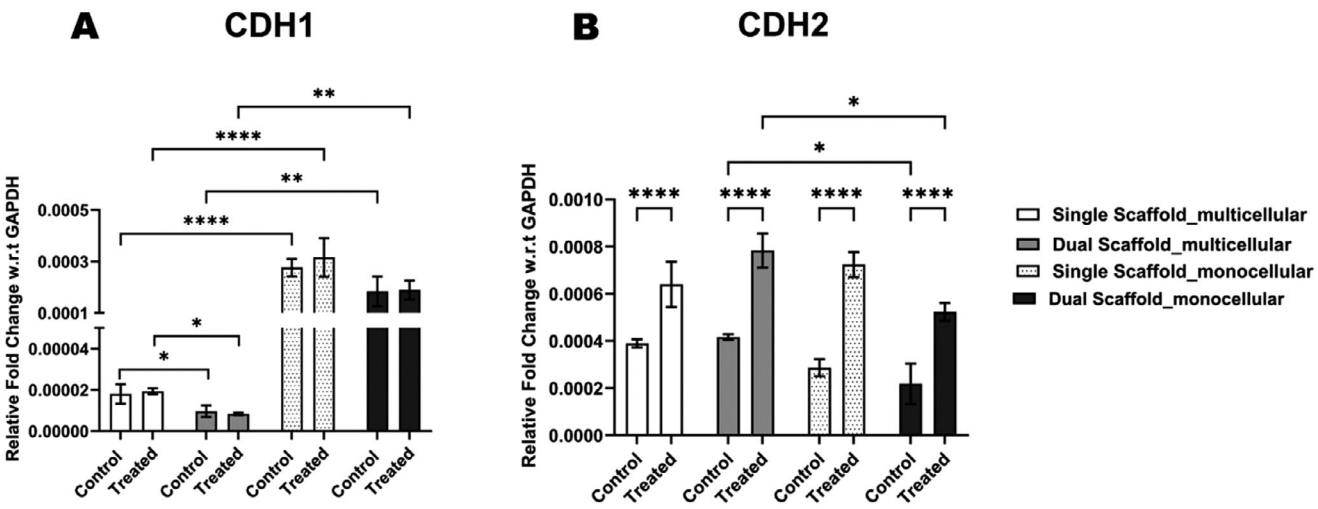

Figure 9. Quantitative analysis of mRNA expression via qPCR for A) E-Cadherin (CDH1) and (B) N-Cadherin (CDH2), in single monocellular, single multicellular, dual monocellular and dual multicellular 3D scaffolds. Data normalized with respect to (w.r.t) GAPDH as housekeeping gene.

(Figure 8C).[37,40] Following post-GEM analysis (24 h after treatment), we consistently observed a substantial decrease in the amount of COL I protein present within the single scaffold a multicellular model (Figure 8E,F,I) with minimal to no effect on COL I levels in the both the inner (Figure 8G,I) and outer (Figure 8H,I) compartments of the dual multicellular scaffold. This can be attributed to cellular death of all three cell types including PS-1 stellate cells within the monocellular model as observed previously in Figures 2 and 6. As COL I is interstitial, death and consequent removal (wash-out) of the stellate cells in the single scaffold can also lead to the wash-out of the interstitial collagen produced in the single scaffold.

3.4. mRNA Expression Analysis within Single and Dual Scaffolds

As described in Section 2.10, an array of qPCR based mRNA expression analysis was carried out to assess the expression levels of the following: i) the epithelial marker E-Cadherin (CDH1), ii) the mesenchymal marker N-Cadherin (CDH2), iii) the ECM protein COL I, iv) the ECM degrading metalloproteinases (MMPs), MMP2 and MMP9, v) the hypoxia inducible factor, HIF1-α and vi) the angiogenic factor VEGF-A. Analysis took place for all scaffold conditions under study both pre- and post-GEM treatment.

As expected, pre-GEM treatment, the epithelial marker E-Cadherin (CDH1), was downregulated in the presence of stromal cells irrespective of the scaffold configuration (both single and dual) (**Figure 9**). Interestingly, the dual scaffold multicellular model showed a significant decrease in the expression levels of CDH1 in comparison to the single scaffold multicellular model; these trends were observed both pre- and post-GEM treatment. Furthermore, in contrast to CDH1 expression, only the dual scaffold multicellular model showed a significant increase in the expression levels of the mesenchymal marker N-Cadherin (CDH2) when compared to its monocellular counterpart (dual scaffold monocellular). These data highlight the importance of spatial separation of the stromal and cancer cells. CDH2 was also upregulated post-GEM treatment in all scaffold configurations under study.

Next, we analyzed the expression of the ECM protein Collagen I (COL I) and the ECM degrading matrix metalloproteinases MMP2 and MMP9. All three markers consistently showed significantly higher expression in the presence of stromal cells when compared to monocellular models, for both single and dual scaffolds (**Figure 10**) pre- and post-GEM treatment. Interestingly, for the multicellular models, we observed significantly higher expression of all three (COL I, MMP2, MMP9) markers in the dual multicellular scaffold, as compared to the single multicellular scaffold (Figure 10), highlighting the impact of spatial segregation on the upregulation of those markers. Post-GEM treatment, only an increase on the expression of MMP9 was observed, as compared to the untreated samples, suggesting a role in GEM resistance within our models.

Then, we evaluated the levels of hypoxia inducing factor 1 α (HIF1-α), which has been linked previously to PDAC's resistance to GEM.[62–64] Pre-GEM treatment we observed a significant increase in HIF1-α expression within our dual multicellular scaffold model as compared to the single multicellular scaffold (**Figure 11**). In addition, we detected an increase in HIF1-α expression post-GEM treatment for all scaffold configurations under study (Figure 11).

Finally, we assessed vascular endothelial growth factor A (VEGF-A), which is a known hypoxia response protein,[65,66] as well as a marker for GEM chemoresistance.[67] As shown in Figure 11, an increase in the expression levels of VEGF-A was observed within our model in the presence of stromal cells, irrespective of the cellular spatial arrangement (for both single and dual scaffolds). Furthermore, an increased VEGF-A expression was also observed post-GEM treatment for all scaffold configurations under study (Figure 11).

4. Discussion

Overall, we have performed a systematic study of the changes in cellular characteristics and chemotherapy (GEM) response in

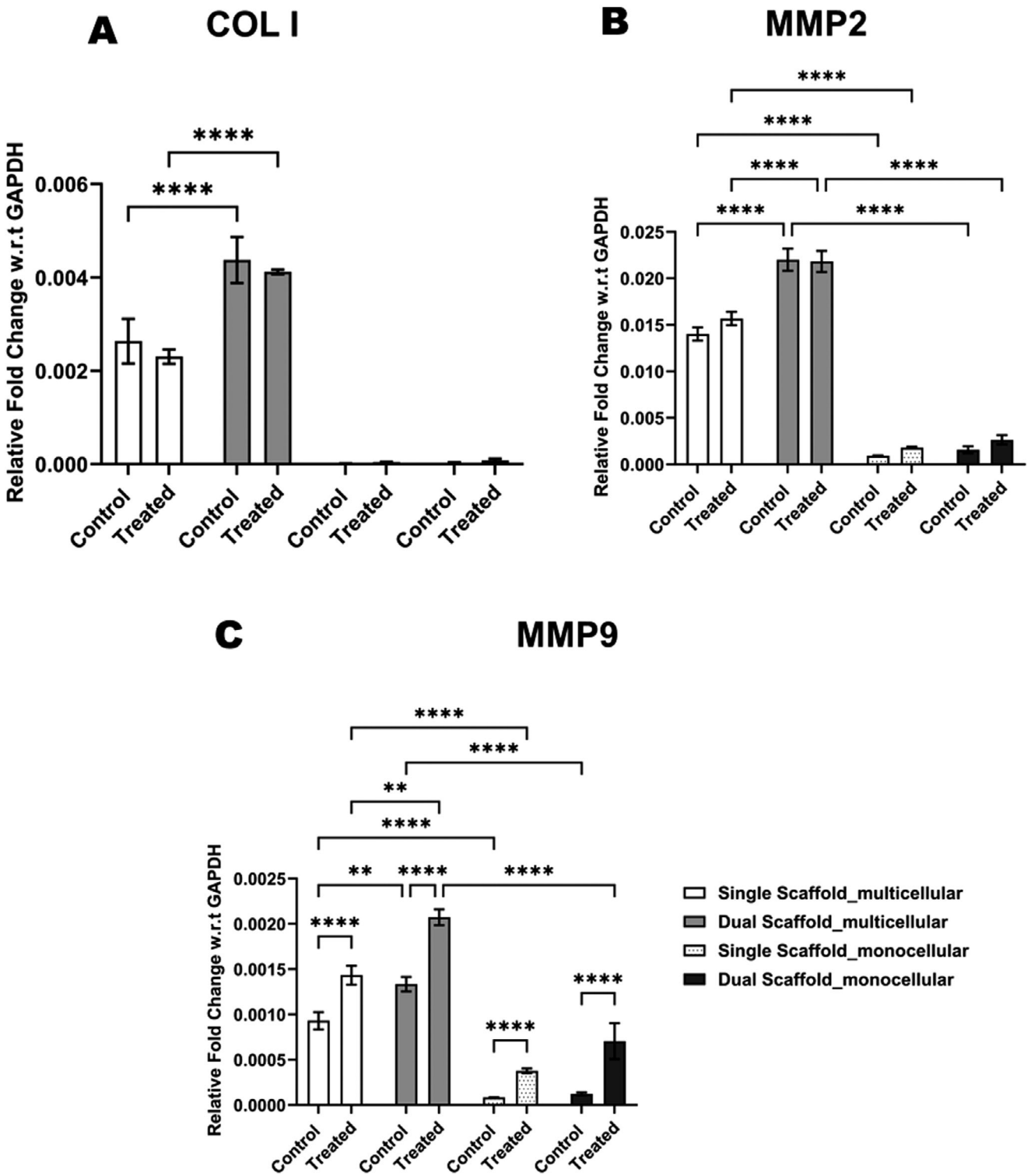

Figure 10. Quantitative analysis of mRNA expressions via qPCR for A) Collagen1 (COL1)), B) matrix metalloproteinases (MMPs) 2 (MMP2) and C) 9 (MMP9), in single monocellular, single multicellular, dual monocellular and dual multicellular 3D scaffolds. Data normalized with respect to (w.r.t) GAPDH as housekeeping gene.

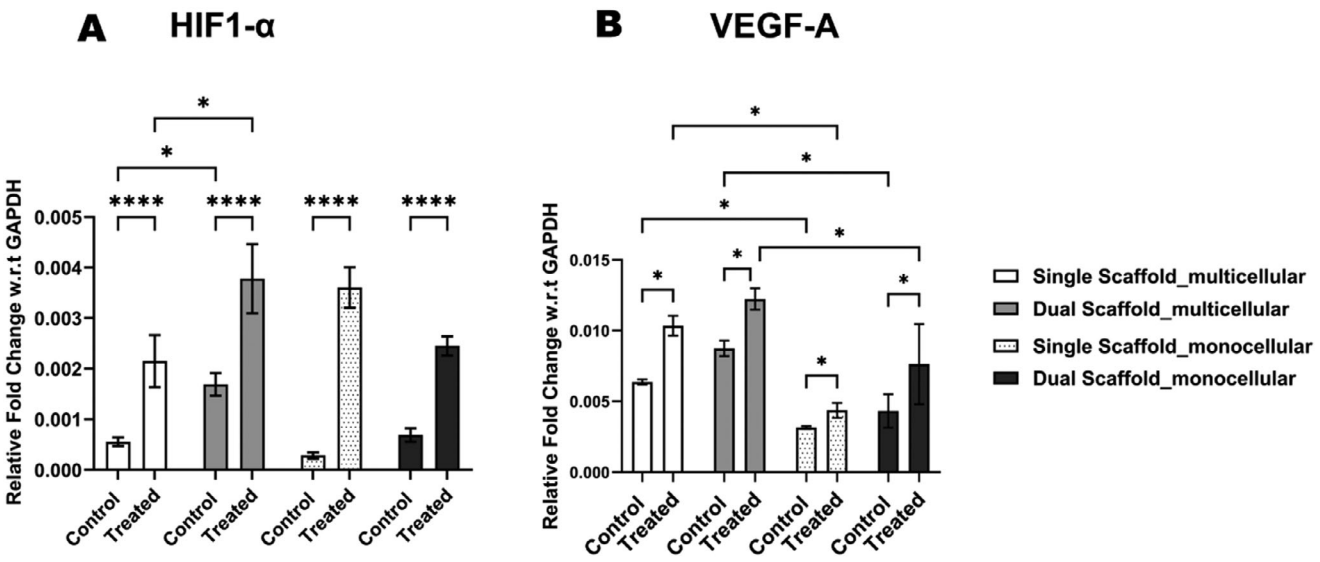

Figure 11. Quantitative analysis of mRNA expressions via qPCR for A) hypoxia inducing factor (HIF1α), and B) vascular endothelial growth factor A(VEGF-A), in single monocellular, single multicellular, dual monocellular and dual multicellular 3D scaffolds. Data normalized with respect to (w.r.t) GAPDH as housekeeping gene.

single and dual polymeric scaffold monocellular and multicellular PDAC models (Figure 1). Comparative analysis, for all scaffold configurations pre- and post-GEM treatment, was carried out i) at the protein level via Live-Dead assay (Figures 2 and 4), Caspase 3/7 activity (Figures 3 and 5), cell specific marker spatial analysis (Figures 6 and 7) and COL I spatial protein secretion (Figure 8), and ii) at mRNA level via qPCR based mRNA expression analysis of markers related to GEM resistance (Figures 9–11).

Our findings highlight the importance of i) stromal cells (activated stellate cells and endothelial cells) as well as ii) cell segregation (spatial compartmentalization of different cell types in separate scaffold compartments, to better mimic the in vivo spatial architecture of the PDAC niche) in promoting resistance against GEM.

4.1. Single Scaffold Monocellular and Multicellular Models: The Importance of the Incorporation of Stromal Cells

In the current work, first, single PU scaffold models were developed, both multicellular and monocellular (Figure 1 and Section 2.3.1). As evident from the decreased post-GEM treatment cellular viability (Figure 2) and increased apoptotic cell numbers in the single monocellular scaffolds (Figure 3), as compared to single multicellular scaffolds, the presence of stromal cells did not lead to chemoresistance against GEM, at least 24 h post-GEM treatment. There are no other studies in literature on polymeric based macroporous scaffolds, however, there are reports on chemotherapy treatment in multicellular spheroid or hydrogel based PDAC models. For example it has been shown that the presence of stellate cells or CAFs, resulted in reduced diffusion of drugs (gemcitabine and paclitaxel) within PDAC (PANC-1) spheroids.[68] Furthermore, higher chemoresistance to chemotherapeutic reagents like gemcitabine, oxaliplatin and paclitaxel was also observed in multicellular PDAC and hydrogel models in the presence of CAFs.[52,53] The differences in the trends observed in our single multicellular and monocellular scaffolds, as compared to currently published hydrogel or spheroid based models, can be attributed to the presence of less diffusional limitations of GEM as well as inherent differences within the cellular population due to specific scaffold characteristics.[6,69,70]

To assess the evolution of different cell types (PANC-1, PS-1 and HMEC) within the single multicellular scaffold, IF imaging with cell specific markers took place via CLSM. As, observed in Figure 6A–C after 4 weeks in culture (and pre-GEM treatment), repetitive patterns of heterogenous cell specific "micro-niches" were observed within the model, similar to in vivo PDAC tumors, wherein neoplastic cancer cell masses are embedded within the stromal cell niche but form their own microenvironment.[71–73] The most important observation was the overall decrease in stellate cell population and an increased presence of HMEC post-chemotherapy, especially in stellate cell rich areas (Figure 6D,E), which suggests that: i) PS-1 stellate cells were affected by chemotherapy and ii) endothelial cells present in densely populated by stellate cells microniches within our single scaffold model showed reduced proliferation pre-chemotherapy, a trend that was reversed post-chemotherapy treatment (most likely as a result of the removal of the stellate cells) (Figure 6D,E). There are very few studies that have investigated the effect of stellate cells on endothelial cells and their function within the PDAC TME. Some groups have reported that activated pancreatic stellate cells secrete both pro- and anti-angiogenic factors like VEGF, angiopoietin-1, endostatin and vasohibin-1 and have a complex role in promoting and suppressing the endothelial cells within the TME.[74–76] However, to the best of our knowledge, we are the first to report such a direct relation between endothelial cell growth suppression/promotion in presence of stellate cells as well as the role of chemotherapy on this balance within a 3D in vitro PDAC model. Further studies to better understand

this interesting phenomenon could shed light on the effects of therapeutic methods on PDAC's stromal components.

Analysis of human specific Collagen I (COL I) protein secretion within our single scaffold multicellular model (Figure 8A,B,E,F) was carried out to assess the presence of fibrosis/desmoplasia in this model, pre- and post-GEM treatment. After 4 weeks of culture (and pre-GEM treatment), we observed some heterogeneity in COL I presence within our models, likely because of the heterogenous distribution of the stellate cells. However, generally we observe substantial amounts of COL I present within the single scaffold, primarily secreted by the stellate cells (Figure 8A). However, post-GEM treatment, decreased amount of COL I protein on the scaffolds was observed (Figure 8E,F). Alvarez et al., reported similar observations in vivo in a clinical study, i.e., a decreased collagen content along with reduced CAFs in a combined treatment involving nab-paclitaxel and gemcitabine, but attributed it as a result of the presence of nab-paclitaxel rather than GEM.[77] A similar observation was also made by Heger et al., in PDAC patient samples.[78] More specifically, the authors performed image-based analysis and quantification of αSMA positive cells and COL I quantity within patient samples post-treatment with a combination of GEM and nab-paclitaxel and calculated the Activated Stroma Index (ASI, ratio of αSMA positive CAFs and volume of COL I deposited). They observed a higher ASI for patients, post-treatment with GEM and nab-paclitaxel when compared to FOLFIRINOX, indicating decreased COL deposition by the fibroblasts in the first treatment combination. To the best of our knowledge, there has been no study to date directly correlating GEM treatment with decreased COL I presence in PDAC in vitro models. However, the role of COL I ECM protein itself to GEM resistance in PDAC has been reported previously by Dangi-Garimella et al. The authors showed that PANC-1 and AsPC-1 pancreatic cancer cells grown in 3D collagen gels exhibited enhanced resistance to GEM treatment in comparison to 2D culture.[79,80] Generally, targeting activated pancreatic stellate cells to reduce their ECM secretion and invasive nature has been reported to be an effective method to increase the efficacy of chemotherapeutic agents including GEM previously.[81,82] Therefore, the heterogeneity in PS-1 distribution along with reduced COL I in stellate cell poor areas of the single scaffold could be a contributing factor towards our observed lack of chemoresistance. Post-GEM treatment, as COL I is an interstitial protein primarily secreted by PS-1 cells which are impacted and likely washed out from the scaffold (dead cells), it is likely that the COL-I is being also removed/washed out along them.

Further elucidation of the PDAC cancer cells' interaction with stromal cells in our single scaffolds was carried out through mRNA expression analysis of various markers via q-PCR. As evident in Figure 9, the presence of stromal cells (specifically the stellate cells), significantly decreased the expressions of epithelial markers E-Cadherin (CDH1) within our model, as reported previously by other groups for other in vitro models of co-culture of cancer cells and stellate cells/CAFs.[58,83–87] Surprisingly, we did not observe any corresponding increase in the expression of mesenchymal marker N-Cadherin (CDH2) pre-treatment within our single multicellular scaffold model, which contradicts several published findings in other in vitro models.[85,88] However, a similar observation of decreased expression of E-Cadherin without any subsequent increase in N-Cadherin was observed by Joost et al.[89] Post-GEM treatment, we observed an increase in mRNA expression of N-Cadherin in both monocellular and multicellular single scaffold models, in accordance with literature.[90–92]

Analysis of the collagen I (COL I) mRNA expression levels 4 weeks in culture (pre-GEM treatment), showed a significant increase in COL I in the multicellular single scaffold as compared to the monocellular single scaffold (Figure 10) in accordance with our CLSM imaging (Figure 8), re-confirming the role of the stellate cells in ECM secretion and promotion of desmoplasia within the PDAC TME.[93–97] However, no change was observed in COL I quantity post-GEM treatment at the mRNA level (Figure 10), strengthening our hypothesis that COL I was not found in the single scaffolds post-treatment likely because of washing-out/removal along with dead stellate cells. Additionally, significant upregulation of the mRNA expression of MMP2 and MMP9 after 4 weeks in culture (and pre-GEM treatment) was observed in the single multicellular scaffolds as compared to the single monocellular scaffolds (Figure 10). Matrix metalloproteinases are known to have significant role in ECM remodeling, cancer metastasis and even resistance to chemotherapy in pancreatic cancer.[98–103] Our results are in accordance with other published studies, with a general consensus in literature that, in addition to the cancer cells, stellate cells contribute heavily to the secretion of both MMP2 and MMP9 within in vivo and in vitro multicellular PDAC models.[38,99,104–106] Post-GEM treatment, a significant increase in the expression of MMP9 was observed for both the monocellular and the multicellular single scaffold models. Our observations are in alignment with previously published work by Wang et al., wherein increased expression of MMP9 was reported for GEM resistant cell lines in 2D without any increase in MMP2 expression.[107] In addition, Ju et al., (2016), also demonstrated an increase in only MMP9 and not MMP2 in spheroid-based 3D models of PDAC (PANC-1, AsPC-1 an MiaPACa-2) post-GEM treatment.[108] Collectively, both the available literature and our data suggest that MMP9 and not MMP2 plays a role in GEM resistance in PDAC.

The presence of the stromal cells also significantly increased the expression of VEGF-A within our single scaffold model after 4 weeks in culture (Figure 11). Both cancer cells and stromal cells are known to secrete VEGF-A, and several studies have shown an increase in VEGF-A expression in multicellular PDAC models.[85,95,109] Furthermore, VEGF-A expression levels were significantly upregulated post-GEM treatment, in both the monocellular and the multicellular single scaffold models (Figure 11). Such a direct effect of VEGF-A in promoting gemcitabine resistance was also observed by Zhang et al., for MiaPaCa-2 cell line in a 2D culture.[67] We also observed an increased expression of HIF1-α post GEM treatment (Figure 11). The formation of a hypoxic environment has been linked to increased expression of VEGF-A, i.e., a direct link between an increased expression of HIF1-α and the upregulation of the expression of VEGF-A has been reported previously.[65,110,111]

To summarize, we observed significant increase in expression levels of key markers related to cellular phenotype, ECM presence and matrix remodeling, hypoxia and angiogenesis within our single scaffold assisted multicellular model at the protein and mRNA level, highlighting the importance of incorporation of the stromal component. However, these effects were not translated

to increased cancer cell viability post-GEM treatment suggesting that the presence of stromal cells alone was not enough to provide GEM resistance within our scaffold-based system.

4.2. Dual Scaffold Monocellular and Multicellular Models: The Importance of Segregation/Compartmentalization and Mimicry of the Spatial Architecture of the Pancreatic Tumor Microenvironment

To assess the impact of cell spatial separation/segregation (in a manner that mimics the in vivo PDAC microenvironment from an architectural point of view) on the cellular phenotype and post-GEM treatment response, we compared our previously developed dual multicellular scaffold a model[37] to: i) a dual monocellular (cancer only) scaffold model and ii) a single multicellular scaffold model (the latter discussed in Section 4.1, see also Figure 1). As observed in Figure 4, the cell viability in both the cancer (PANC-1) and stromal (PS-1, HMEC) compartment was not affected post-GEM treatment in the dual multicellular scaffold, in contrast to the monocellular dual scaffold model (Figure 4) and the single multicellular scaffold (Figure 2). Measurement of Caspase 3/7 positive apoptotic cells showed significant increase post-GEM treatment for the dual monocellular scaffold as well as for both the cancer and stromal compartments within the dual multicellular scaffold (Figure 5). However, interestingly the apoptotic cell number was significantly lower within the inner (cancer) compartment of the dual multicellular scaffold as compared to the outer (stroma) compartment and the dual monocellular scaffold (Figure 5). Collectively, our data suggest that both the mimicry of the spatial arrangement as well as the presence of the stromal cells (primarily the stellate cells) were important for the development of GEM resistance (resulting in delayed cell death) in our scaffolds. Hessmann et al., in their landmark paper have demonstrated that CAFs and pancreatic stellate cells showed significantly higher intracellular concentrations of gemcitabine metabolites, in comparison to tumor cell lines derived from primary murine PDAC and metastases.[112] Their hypothesis that the tumor fibroblasts scavenge GEM within them and reduce its delivery to tumor cells supports our observation of chemotherapeutic resistance within the cancer compartment of our dual multicellular scaffold. In addition, as discussed in Section 1, the importance of cell (stroma) compartmentalization on increasing the chemotherapy resistance of PANC-1, has been recently demonstrated by Monteiro et al., in their novel "cancer on bead" hydrogel-based 3D model.[50]

As previously discussed, cell specific markers spatial analysis of the dual multicellular scaffold was carried out at week 4 of culture as well as 24 hours post-GEM treatment (Section 2.7). As observed in Figure 7, PANC-1 and PS-1 cells mostly resided within their specific compartments after 4 weeks in culture. Within the stromal compartment, excessive number of stellate cells seemed to have pushed the endothelial cells to the periphery of the model (Figure 7D). Interestingly, a significant presence of endothelial cells was observed within the cancer compartment (Figure 7B,E,F), and presence of cancer cells was observed in the stroma compartment (Figure 7C,D,G,H) demonstrating cellular movement within our dual multicellular scaffold model. Post-GEM treatment, we did not observe any discernible changes in the cell density and distribution within the cancer compartment of the dual multicellular scaffold (Figure 7E,F). However, within the stromal compartment, loss of αSMA and fibroblastic spindle shape of the stellate cells was observed, further supporting our hypothesis that the stellate cells are entrapping the GEM within the stromal compartment (Figure 7G,H).

Analysis of cellular spatial deposition of COL I at the protein level, highlighted that i) there was excessive COL I in the outer compartment of the dual multicellular scaffold at 4 weeks of culture (pre-GEM treatment) and that (ii) there was no discernible change in the COL I quantity/density post-GEM treatment within the two compartments of the dual multicellular scaffold (Figure 8C,D,G,H). This contradicts the trend we observed in the single multicellular scaffold wherein COL I was depleted post-GEM treatment (Figure 7D). The role of excessive stromal COL I (desmoplasia) in the PDAC's treatment resistance is well documented.[113–116] For example, Khan et al. reported that combining GEM treatment with Ormeloxifene (known to deplete tumor associated desmoplasia through inhibition of Sonic Hedgehog pathway) potentiated the antitumorigenic effect of gemcitabine by 75% in PDAC xenograft mice.[114] These observations suggested that the chemoresistance to GEM within our dual scaffold multicellular model could be attributed to the dense desmoplastic/fibrotic reaction surrounding the cancer mass. Further to better retention of COL I post-treatment, the stellate cells are less affected by GEM as compared to the single multicellular scaffold (Figures 6 and 7) collectively indicating a denser fibrotic formation in the dual multicellular scaffold, as compared to the single monocellular scaffold.

Similar to the single scaffold models, q-PCR based analysis of mRNA expression of different biomarkers was carried out. As demonstrated in Figure 9, following 4 weeks in culture, a significant decrease in expression levels of the epithelial marker E-Cadherin (CDH1) along with an increase in the expression of the mesenchymal marker N-Cadherin (CDH2) were observed within the dual multicellular model as compared to the dual monocellular scaffold. This was in contrast to our single scaffold model, wherein the presence of stromal cells significantly lowered the expression level of CDH1 only with no concomitant increase in CDH2 (Figure 9). A similar depletion of CDH1 expression for PANC-1 cells when co-cultured with stellate cells was also reported by Norberg et al., within their heterotypic spheroid mode of PDAC.[87] Interestingly, they did not see a similar complete depletion of CDH1 with the HPAFII PDAC cell line, suggesting these changes can be cell specific. Collectively, these data, suggest that the compartmentalization/segregation of the stroma and cancer cells have significant impact in the response of cancer cells to chemotherapy within our scaffolds. Further studies are required to elucidate the mechanism behind these observations. Post-GEM treatment, similar to our observations for the single monocellular and multicellular scaffolds, we observed increased expressions of N-Cadherin in both our monocellular and multicellular scaffolds (Figure 9), suggesting that the surviving population has higher numbers of mesenchymal cell-like properties (see also discussion in Section 4.1).

In alignment with our observations for the single scaffolds and with published literature (see Section 4.1), increased expression levels of COL I, MMP2 and MMP9 were observed within the dual multicellular scaffolds as compared to the dual

monocellular scaffolds, after 4 weeks in culture (and pre-GEM treatment) (Figure 10). Interestingly, we observed significantly higher expressions for COL I, MMP2 and MMP9 within our dual multicellular scaffold, as compared to the single multicellular scaffold (Figure 10). The importance of COL I, MMP2 and MMP9 in modulating chemoresistance to PDAC is well documented[108,116–121] and their upregulation within our dual scaffold model further supports our observed resistance to GEM and the importance of cell spatial arrangement to better map it (Figures 4 and 5).

We observed a significant upregulation of the mRNA expression of VEGF-A within the dual multicellular scaffold, as compared to the dual monocellular scaffold after 4 weeks in culture (Figure 11). Also, after 4 weeks in culture (and pre-GEM treatment), a significantly higher expression of HIF1-α was seen within the dual multicellular scaffold, as compared to the single multicellular scaffold (Figure 11), highlighting once again the importance of cellular spatial segregation. Furthermore, we observed upregulation of VEGF-A and HIF1-α post treatment in both the monocellular and multicellular dual scaffolds (Figure 11). Considering the importance of hypoxia and HIF1-α in promoting chemoresistance,[62–64,122] the difference in its expression between the two scaffold configurations, i.e., dual versus single, further highlights the importance of spatial separation/segregation between the cancer and stromal compartment for better mimicry of chemoresistance.

To summarize, the dual multicellular scaffold showed extensive chemoresistance to GEM in comparison to all other models assessed, i.e., dual and single monocellular as well as single multicellular scaffolds. Additionally, the spatial separation of stromal cells from the PANC-1 cancer cells in the dual multicellular scaffold, resulted in i) significantly higher expression levels of COL1, MMP2, MMP9 and HIF1-α at the mRNA level as compared to the single multicellular scaffold and ii) in no discernible changes in the COL I presence pre and post-GEM treatment (within the dual scaffold multicellular model).

Our data highlight the importance of mimicking the cellular composition as well as the spatial architecture and position of the stromal cells within a 3D in vitro model for better modeling of the PDAC chemoresistance.

5. Conclusion

In this study, we investigated the importance of multicellularity as well as spatiotemporal cellular and matrix modeling on the evolution and treatment response of PDAC in 3D PU scaffolds. More specifically, we performed a systematic comparative study of the PDAC evolution and chemotherapy (GEM) response in: i) our novel zonal/dual multicellular (tri-culture) PU scaffold model[37] ii) a PU zonal/dual monocellular (cancer only) scaffold model consisting of a central cancer mass, surrounded by an external cell-free but ECM rich (COL I) periphery iii) a single PU monocellular scaffold model and iv) a single PU multicellular (tri-culture) scaffold model.

We have demonstrated that our PU scaffold based multicellular PDAC models are capable of mimicking key characteristics associated with the effects of chemotherapy on pancreatic cancer. We have highlighted that, post-treatment with gemcitabine, the surviving cell population reflects an upregulation of mesenchymal, hypoxic and matrix remodeling markers, suggesting a clear pattern towards cellular survival post-treatment for all the scaffold configurations under study. Furthermore, we have also conclusively shown that within our polymeric scaffolds, both multicellularity and appropriate architectural mimicry (through compartmentalization/separation of the cancer and stromal cellular components) are required for demonstrating effective chemoresistance.

Overall, our findings highlight the importance of spatiotemporal design of cellular and matrix components in 3D cancer models. Future work is needed to elucidate the molecular mechanisms of cell–cell interactions behind these interesting observations.

Supporting Information

Supporting Information is available from the Wiley Online Library or from the author.

Acknowledgements

E.G.V. (principal investigator) and P.A.P-M. (co-investigator) are grateful to the Medical Research Council UK for a New Investigator Research Grant (MR/V028553/1), which also financially supports P.G. C.B-R. is supported by NC3Rs (NC/V001167/1). P.G and E.V. also acknowledge previous funding from 3D bioNet UKRI network (MR/R025762/1). The authors dedicate this original research article in memory of their colleague Dr Alan Millington from the University of Surrey UK, who, sadly, passed away after battling pancreatic cancer in March 2022.

Conflict of Interest

The authors declare no conflict of interest.

Author Contributions

P.G.: conception and design of experiments, data collection, data analysis and interpretation, manuscript writing; C.B.R: design of experiment (primer designing), manuscript reviewing; H.K.: provision of materials (PS-1 cell line), manuscript reviewing; P.A.P.M.: conception of research, contribution to the design of experiments, data interpretation, manuscript reviewing, funding acquisition; E.G.V.: conception of research, contribution to the design of experiments, data interpretation, manuscript writing and reviewing, funding acquisition, supervision.

Data Availability Statement

The data that support the findings of this study are available from the corresponding author upon reasonable request.

Keywords

3D model, chemoresistance, gemcitabine, multicellular tumor model, pancreatic cancer, stellate cells

Received: November 3, 2023
Revised: January 10, 2024
Published online:

[1] R. L. Siegel, K. D. Miller, A. Jemal, *Ca-Cancer J. Clin.* **2019**, *69*, 7.
[2] Cancer.net. https://www.cancer.net/cancer-types/pancreatic-cancer/statistics (accessed: September 2019).
[3] J. Kleeff, P. Beckhove, I. Esposito, S. Herzig, P. E. Huber, J. M. Löhr, H. Friess, *Int. J. Cancer* **2007**, *121*, 699.
[4] D. Ansari, H. Friess, M. Bauden, J. Samnegård, R. Andersson, *Oncotarget* **2018**, *9*, 6644.
[5] S. Chand, K. O'Hayer, F. F. Blanco, J. M. Winter, J. R. Brody, *Int. J. Biol. Sci.* **2016**, *12*, 273.
[6] S. Totti, S. I. Vernardis, L. Meira, P. A. Pérez-Mancera, E. Costello, W. Greenhalf, D. Palmer, J. Neoptolemos, A. Mantalaris, E. G. Velliou, *Drug Discovery Today* **2017**, *22*, 690.
[7] A. Seicean, L. Petrusel, R. Seicean, *World J. Gastroenterol.* **2015**, *21*, 6127.
[8] H. Onishi, Y. Morifuji, K. Suyama, H. Iwasaki, M. Katano, *Cancer Sci.* **2012**, *103*, 1272.
[9] J. W. Zhang, F. Zhao, Q. Sun, *Oncol. Lett.* **2018**, *15*, 1811.
[10] C. Serri, V. Quagliariello, R. V. Iaffaioli, S. Fusco, G. Botti, L. Mayol, M. Biondi, *J. Cell. Physiol.* **2019**, *234*, 4959.
[11] Y. Sato, S. Yamada, S. Takeda, N. Hattori, K. Nakamura, H. Tanaka, M. Mizuno, M. Hori, Y. Kodera, *Ann. Surg. Oncol.* **2018**, *25*, 299.
[12] A. Courtin, F. M. Richards, T. E. Bapiro, J. L. Bramhall, A. Neesse, N. Cook, B.-F. Krippendorff, D. A. Tuveson, D. I. Jodrell, *PLoS One* **2013**, *8*, e67330.
[13] N. Awasthi, D. Kronenberger, A. Stefaniak, M. S. Hassan, U. V. Holzen, M. A. Schwarz, R. E. Schwarz, *Cancer Lett.* **2019**, *459*, 41.
[14] S. Shinoda, S. Kaino, S. Amano, H. Harima, T. Matsumoto, K. Fujisawa, T. Takami, N. Yamamoto, T. Yamasaki, I. Sakaida, *Oncotarget* **2018**, *9*, 28434.
[15] T. M. Pausch, E. Aue, N. M. Wirsik, A. Freire Valls, Y. Shen, P. Radhakrishnan, T. Hackert, M. Schneider, T. Schmidt, *Sci. Rep.* **2020**, *10*, 5420.
[16] G. Obaid, S. Bano, S. Mallidi, M. Broekgaarden, J. Kuriakose, Z. Silber, A.-L. Bulin, Y. Wang, Z. Mai, W. Jin, D. Simeone, T. Hasan, *Nano Lett.* **2019**, *19*, 7573.
[17] K. Doello, C. Mesas, F. Quiñonero, G. Perazzoli, L. Cabeza, J. Prados, C. Melguizo, R. Ortiz, *Cancers* **2021**, *13*, 3169.
[18] A. F. Adcock, G. Trivedi, R. Edmondson, C. Spearman, L. Yang, *J. Anal. Bioanal. Tech.* **2015**, *6*, 2.
[19] L. K. Chim, A. G. Mikos, *Curr. Opin. Biomed. Eng.* **2018**, *6*, 42.
[20] L. R. Jaidev, U. M. Krishnan, S. Sethuraman, *Mater. Sci. Eng., C* **2015**, *47*, 40.
[21] C. Bermejo-Rodríguez, P. A. Pérez-Mancera, *Curr. Opin. Biotechnol.* **2015**, *35*, 103.
[22] D. J. Erstad, M. Sojoodi, M. S Taylor, S. Ghoshal, A. A Razavi, K. A. Graham-O'Regan, N. Bardeesy, C. R. Ferrone, M. Lanuti, P. Caravan, K. K Tanabe, B. C. Fuchs, *Dis. Models Mech.* **2018**, *11*, dmm034793.
[23] T. J. Humpton, B. Alagesan, G. M. DeNicola, D. Lu, G. N. Yordanov, C. S. Leonhardt, M. A Yao, P. Alagesan, M. N. Zaatari, Y. Park, J. N. Skepper, K. F. Macleod, P. A Perez-Mancera, M. P. Murphy, G. I. Evan, K. H. Vousden, D. A. Tuveson, *Cancer Discovery* **2019**, *9*, 1268.
[24] X. Yan, L. Zhou, Z. Wu, X. Wang, X. Chen, F. Yang, Y. Guo, M. Wu, Y. Chen, W. Li, J. Wang, Y. Du, *Biomaterials* **2018**, *198*, 167.
[25] L. Ireland, A. Santos, M. S. Ahmed, C. Rainer, S. R. Nielsen, V. Quaranta, U. Weyer-Czernilofsky, D. D. Engle, P. A. Perez-Mancera, S. E. Coupland, A. Taktak, T. Bogenrieder, D. A. Tuveson, F. Campbell, M. C. Schmid, A. Mielgo, *Cancer Res.* **2016**, *76*, 6851.
[26] P. A. Pérez–Mancera, C. Guerra, M. Barbacid, D. A. Tuveson, *Gastroenterology* **2012**, *142*, 1079.
[27] D. Xie, S. Jia, D. Ping, D. Wang, L. Cao, *Cytotechnology* **2022**, *74*, 657.
[28] K. O. Affram, T. Smith, E. Ofori, S. Krishnan, P. Underwood, J. G. Trevino, E. Agyare, *J. Drug Delivery Sci. Technol.* **2020**, *55*, 101374.
[29] P. Longati, X. Jia, J. Eimer, A. Wagman, M.-R. Witt, S. Rehnmark, C. Verbeke, R. Toftgård, M. Löhr, R. L. Heuchel, *BMC Cancer* **2013**, *13*, 95.
[30] C. S. Ki, H. Shih, C.-C. Lin, *Biomacromolecules* **2013**, *14*, 3017.
[31] X. Liu, B. Gündel, X. Li, J. Liu, A. Wright, M. Löhr, G. Arvidsson, R. Heuchel, *Transl. Oncol.* **2021**, *14*, 101107.
[32] I. Dufau, C. Frongia, F. Sicard, L. Dedieu, P. Cordelier, F. Ausseil, B. Ducommun, A. Valette, *BMC Cancer* **2012**, *12*, 15.
[33] J. Pape, K. Stamati, R. Al Hosni, I. F. Uchegbu, A. G. Schatzlein, M. Loizidou, M. Emberton, U. Cheema, *Int. J. Mol. Sci.* **2021**, 4289, *22*.
[34] P. Gupta, S. Totti, P. A. Pérez-Mancera, E. Dyke, A. Nisbet, G. Schettino, R. Webb, E. G. Velliou, *RSC Adv.* **2019**, *9*, 41649.
[35] C. R. Below, J. Kelly, A. Brown, J. D. Humphries, C. Hutton, J. Xu, B. Y. Lee, C. Cintas, X. Zhang, V. Hernandez-Gordillo, L. Stockdale, M. A. Goldsworthy, J. Geraghty, L. Foster, D. A. O'Reilly, B. Schedding, J. Askari, J. Burns, N. Hodson, D. L. Smith, C. Lally, G. Ashton, D. Knight, A. Mironov, A. Banyard, J. A. Eble, J. P. Morton, M. J. Humphries, L. G. Griffith, C. Jørgensen, *Nat. Mater.* **2022**, *21*, 110.
[36] M. C. Allenby, N. Panoskaltsis, A. Tahlawi, S. B. D. Santos, A. Mantalaris, *Biomaterials* **2019**, *188*, 24.
[37] P. Gupta, P. A. Pérez-Mancera, H. Kocher, A. Nisbet, G. Schettino, E. G. Velliou, *Front. Bioeng. Biotechnol.* **2020**, *8*, https://doi.org/10.3389/fbioe.2020.00290.
[38] C. Ricci, C. Mota, S. Moscato, D. D'Alessandro, S. Ugel, S. Sartoris, V. Bronte, U. Boggi, D. Campani, N. Funel, L. Moroni, S. Danti, *Biomatter* **2014**, *4*, e955386.
[39] G. Wishart, P. Gupta, A. Nisbet, G. Schettino, E. Velliou, *Cancers* **2021**, 6080, *13*.
[40] S. Totti, M. C. Allenby, S. B. D. Santos, A. Mantalaris, E. G. Velliou, *RSC Adv.* **2018**, *8*, 20928.
[41] S. Hamada, A. Masamune, T. Takikawa, N. Suzuki, K. Kikuta, M. Hirota, H. Hamada, M. Kobune, K. Satoh, T. Shimosegawa, *Biochem. Biophys. Res. Commun.* **2012**, *421*, 349.
[42] R. R. Bynigeri, A. Jakkampudi, R. Jangala, C. Subramanyam, M. Sasikala, G. V. Rao, D. N. Reddy, R. Talukdar, *World J. Gastroenterol.* **2017**, *23*, 382.
[43] E. Karnevi, A. H. Rosendahl, K. S. Hilmersson, M. A. Saleem, R. Andersson, *Exp. Cell Res.* **2016**, *346*, 206.
[44] D. Wang, Y. Li, H. Ge, T. Ghadban, M. Reeh, C. Güngör, *Cancers* **2022**, *14*, 3998.
[45] V. M. Perez, J. F. Kearney, J. J. Yeh, *Front. Oncol.* **2021**, *11*, 751311.
[46] V. Fernandez-Vega, S. Hou, D. Plenker, H. Tiriac, P. Baillargeon, J. Shumate, L. Scampavia, J. Seldin, G. R. Souza, D. A. Tuveson, T. P. Spicer, *SLAS Discovery* **2022**, *27*, 159.
[47] O. Firuzi, P. P. Che, B. El Hassouni, M. Buijs, S. Coppola, M. Löhr, N. Funel, R. Heuchel, I. Carnevale, T. Schmidt, G. Mantini, A. Avan, L. Saso, G. J. Peters, E. Giovannetti, *Cancers* **2019**, *11*, 638.
[48] S. Hahn, B. J. Oh, H. Kim, I. W. Han, S. H. Shin, G. Kim, S.-M. Jin, J. H. Kim, *Am. J. Cancer Res.* **2023**, *13*, 1806.
[49] G. Lazzari, V. Nicolas, M. Matsusaki, M. Akashi, P. Couvreur, S. Mura, *Acta Biomater.* **2018**, *78*, 296.
[50] M. V. Monteiro, M. Rocha, V. M. Gaspar, J. F. Mano, *Adv. Healthcare Mater.* **2022**, *11*, 2102574.
[51] M. Broekgaarden, S. Anbil, A.-L. Bulin, G. Obaid, Z. Mai, Y. Baglo, I. Rizvi, T. Hasan, *Biomaterials* **2019**, *222*, 119421.
[52] D. Osuna de la Peña, S. M. D. Trabulo, E. Collin, Y. Liu, S. Sharma, M. Tatari, D. Behrens, M. Erkan, R. T. Lawlor, A. Scarpa, C. Heeschen, A. Mata, D. Loessner, *Nat. Commun.* **2021**, *12*, 5623.
[53] R. Curvello, V. Kast, M. H. Abuwarwar, A. L. Fletcher, G. Garnier, D. Loessner, *Front. Digital Health* **2021**, *3*, 704584.
[54] D. F. Mardhian, A. Vrynas, G. Storm, R. Bansal, J. Prakash, *Nanotheranostics* **2020**, *4*, 26.
[55] M. J. Ware, V. Keshishian, J. J. Law, J. C. Ho, C. A. Favela, P. Rees, B. Smith, S. Mohammad, R. F. Hwang, K. Rajapakshe, C. Coarfa, S.

Huang, D. P. Edwards, S. J. Corr, B. Godin, S. A. Curley, *Biomaterials* **2016**, *108*, 129.
[56] E. G. Velliou, S. B. Dos Santos, M. M. Papathanasiou, M. Fuentes-Gari, R. Misener, N. Panoskaltsis, E. N. Pistikopoulos, A. Mantalaris, *Bioprocess Biosyst. Eng.* **2015**, *38*, 1589.
[57] N. F. Li, H. M. Kocher, M. A. Salako, E. Obermueller, J. Sandle, F. Balkwill, *Oncogene* **2009**, *28*, 773.
[58] F. E. M. Froeling, T. A. Mirza, R. M. Feakins, A. Seedhar, G. Elia, I. R. Hart, H. M. Kocher, *Am. J. Pathol.* **2009**, *175*, 636.
[59] P. Gupta, E. G. Velliou, in *Cancer Cell Culture: Methods and Protocols* (Eds: D. Movia, A. Prina–Mello), Springer, Berlin **2023**, pp. 221–229.
[60] J. F. Huggett, C. A. Foy, V. Benes, K. Emslie, J. A. Garson, R. Haynes, J. Hellemans, M. Kubista, R. D. Mueller, T. Nolan, M. W. Pfaffl, G. L. Shipley, J. Vandesompele, C. T. Wittwer, S. A. Bustin, *Clin. Chem.* **2013**, *59*, 892.
[61] T. D. Schmittgen, K. J. Livak, *Nat. Protoc.* **2008**, *3*, 1101.
[62] R. Wang, L. Cheng, J. Xia, Z. Wang, Q. Wu, Z. Wang, *Curr. Cancer Drug Targets* **2014**, *14*, 407.
[63] X. Jin, L. Dai, Y. Ma, J. Wang, Z. Liu, *Cancer Cell Int.* **2020**, *20*, 273.
[64] K. Yokoi, I. J. Fidler, *Clin. Cancer Res.* **2004**, *10*, 2299.
[65] N. Gupta, J. E. Park, W. Tse, J. K. Low, O. L. Kon, N. McCarthy, S. K. Sze, *Oncotarget* **2019**, *10*, 5970.
[66] H. Zhang, K. Cao, J. Xiang, M. Zhang, M. Zhu, Q. Xi, *Cancer Lett.* **2023**, *571*, 216345.
[67] Z. Zhang, S. Ji, Q. Hu, Q. Zhuo, W. Liu, W. Xu, W. Liu, M. Liu, Z. Ye, G. Fan, X. Xu, X. Yu, Y. Qin, *Clin. Transl. Med.* **2021**, *11*, e398.
[68] H. J. Hwang, M.-S. Oh, D. W. Lee, H.-J. Kuh, *J. Exp. Clin. Cancer Res.* **2019**, *38*, 1.
[69] E. Velliou, P. Gupta, C. Ricci, S. Danti, in *Biomaterials for 3D Tumor Modeling* (Eds: S. C. Kundu, R. L. Reis), Elsevier, Amsterdam **2020**, pp. 235–249.
[70] M. J. Ware, K. Colbert, V. Keshishian, J. Ho, S. J. Corr, S. A. Curley, B. Godin, *Tissue Eng., Part C* **2016**, *22*, 312.
[71] A. Neesse, H. Algül, D. A. Tuveson, T. M. Gress, *Gut* **2015**, *64*, 1476.
[72] C. Neuzillet, A. Tijeras-Raballand, C. Ragulan, J. Cros, Y. Patil, M. Martinet, M. Erkan, J. Kleeff, J. Wilson, M. Apte, M. Tosolini, A. S. Wilson, F. R. Delvecchio, C. Bousquet, V. Paradis, P. Hammel, A. Sadanandam, H. M. Kocher, *J. Pathol.* **2019**, *248*, 51.
[73] A. N. Hosein, R. A. Brekken, A. Maitra, *Nat. Rev. Gastroenterol. Hepatol.* **2020**, *17*, 487.
[74] R. Brammer, S. Bramhall, M. Eggo, *Br. J. Cancer* **2005**, *92*, 89.
[75] M. B. Patel, S. P. Pothula, Z. Xu, A. K. Lee, D. Goldstein, R. C. Pirola, M. V. Apte, J. S. Wilson, *Carcinogenesis* **2014**, *35*, 1891.
[76] A. Masamune, K. Kikuta, T. Watanabe, K. Satoh, M. Hirota, T. Shimosegawa, *Am. J. Physiol.-Gastrointest. Liver Physiol.* **2008**, *295*, G709.
[77] R. Alvarez, M. Musteanu, E. Garcia-Garcia, P. P. Lopez-Casas, D. Megias, C. Guerra, M. Muñoz, Y. Quijano, A. Cubillo, J. Rodriguez-Pascual, C. Plaza, E. de Vicente, S. Prados, S. Tabernero, M. Barbacid, F. Lopez-Rios, M. Hidalgo, *Br. J. Cancer* **2013**, *109*, 926.
[78] U. Heger, A. Martens, L. Schillings, B. Walter, D. Hartmann, U. Hinz, T. Pausch, N. Giese, C. W. Michalski, T. Hackert, *Cancers* **2022**, *14*, 3881.
[79] S. Dangi-Garimella, S. B. Krantz, M. R. Barron, M. A. Shields, M. J. Heiferman, P. J. Grippo, D. J. Bentrem, H. G. Munshi, *Cancer Res.* **2011**, *71*, 1019.
[80] S. Dangi-Garimella, V. Sahai, K. Ebine, K. Kumar, H. G. Munshi, *PLoS One* **2013**, *8*, e64566.
[81] E. R. Murray, S. Menezes, J. C. Henry, J. L. Williams, L. Alba-Castellón, P. Baskaran, I. Quétier, A. Desai, J. J. T. Marshall, I. Rosewell, M. Tatari, V. Rajeeve, F. Khan, J. Wang, P. Kotantaki, E. J. Tyler, N. Singh, C. S. Reader, E. P. Carter, K. Hodivala-Dilke, R. P. Grose, H. M. Kocher, N. Gavara, O. Pearce, P. Cutillas, J. F. Marshall, A. J. M. Cameron, *Cell Rep.* **2022**, *38*, 110227.
[82] E. F. Carapuça, E. Gemenetzidis, C. Feig, T. E. Bapiro, M. D. Williams, A. S. Wilson, F. R. Delvecchio, P. Arumugam, R. P. Grose, N. R. Lemoine, F. M. Richards, H. M. Kocher, *J. Pathol.* **2016**, *239*, 286.
[83] H. Fujita, K. Ohuchida, K. Mizumoto, T. Egami, K. Miyoshi, T. Moriyama, L. Cui, J. Yu, M. Zhao, T. Manabe, M. Tanaka, *Cancer Sci.* **2009**, *100*, 2309.
[84] K. Kikuta, A. Masamune, T. Watanabe, H. Ariga, H. Itoh, S. Hamada, K. Satoh, S. Egawa, M. Unno, T. Shimosegawa, *Biochem. Biophys. Res. Commun.* **2010**, *403*, 380.
[85] D. Tang, D. Wang, Z. Yuan, X. Xue, Y. Zhang, Y. An, J. Chen, M. Tu, Z. Lu, J. Wei, K. Jiang, Y. Miao, *Int. J. Cancer* **2013**, *132*, 993.
[86] O. Al-Assar, F. Demiciorglu, S. Lunardi, M. M. Gaspar-Carvalho, W. G. McKenna, R. M. Muschel, T. B. Brunner, *Radiother. Oncol.* **2014**, *111*, 243.
[87] K. J. Norberg, X. Liu, C. Fernández Moro, C. Strell, S. Nania, M. Blümel, A. Balboni, B. Bozóky, R. L. Heuchel, J. M. Löhr, *BMC Cancer* **2020**, *20*, 475.
[88] B. Hotz, M. Arndt, S. Dullat, S. Bhargava, H.-J. Buhr, H. G. Hotz, *Clin. Cancer Res.* **2007**, *13*, 4769.
[89] S. Joost, L. L. Almada, V. Rohnalter, P. S. Holz, A. M. Vrabel, M. G. Fernandez-Barrena, R. R. McWilliams, M. Krause, M. E. Fernandez-Zapico, M. Lauth, *Cancer Res.* **2012**, *72*, 88.
[90] F. Bremmer, S. Schallenberg, H. Jarry, S. Küffer, S. Kaulfuss, P. Burfeind, A. Strauß, P. Thelen, H. J. Radzun, P. Ströbel, F. Honecker, C. L. Behnes, *Oncotarget* **2015**, *6*, 33426.
[91] B. Weadick, D. Nayak, A. K. Persaud, S. W. Hung, R. Raj, M. J. Campbell, W. Chen, J. Li, T. M. Williams, R. Govindarajan, *Mol. Cancer Ther.* **2021**, *20*, 410.
[92] Y. Su, J. Li, A. K. Witkiewicz, D. Brennan, T. Neill, J. Talarico, G. L. Radice, *Oncogene* **2012**, *31*, 4484.
[93] C.-W. Wong, H.-W. Han, Y.-W. Tien, S.-h. Hsu, *Biomaterials* **2019**, *213*, 119202.
[94] M. V. Apte, S. Park, P. A. Phillips, N. Santucci, D. Goldstein, R. K. Kumar, G. A. Ramm, M. Buchler, H. Friess, J. A. McCarroll, G. Keogh, N. Merrett, R. Pirola, J. S. Wilson, *Pancreas* **2004**, *29*, 179.
[95] H. J. Hwang, M.-S. Oh, D. W. Lee, H.-J. Kuh, *J. Exp. Clin. Cancer Res.* **2019**, *38*, 258.
[96] M. V. Apte, J. S. Wilson, *J. Gastroenterol. Hepatol.* **2012**, *27*, 69.
[97] M. G. Bachem, M. Schünemann, M. Ramadani, M. Siech, H. Beger, A. Buck, S. Zhou, A. Schmid-Kotsas, G. Adler, *Gastroenterology* **2005**, *128*, 907.
[98] A. M. Knapinska, C.-A. Estrada, G. B. Fields, *Prog. Mol. Biol. Transl. Sci.* **2017**, *148*, 339.
[99] V. Ellenrieder, B. Alber, U. Lacher, S. F. Hendler, A. Menke, W. Boeck, M. Wagner, M. Wilda, H. Friess, M. Büchler, G. Adler, T. M. Gress, *Int. J. Cancer* **2000**, *85*, 14.
[100] M. Bloomston, E. E. Zervos, A. S. Rosemurgy, *Ann. Surg. Oncol.* **2002**, *9*, 668.
[101] M. G. Bachem, S. Zhou, K. Buck, W. Schneiderhan, M. Siech, *Langenbeck's Arch. Surg.* **2008**, *393*, 891.
[102] E. J. Slapak, J. Duitman, C. Tekin, M. F. Bijlsma, C. A. Spek, *Biology* **2020**, *9*, 80.
[103] W. J. Ho, E. M. Jaffee, L. Zheng, *Nat. Rev. Clin. Oncol.* **2020**, *17*, 527.
[104] W. Schneiderhan, F. Diaz, M. Fundel, S. Zhou, M. Siech, C. Hasel, P. Möller, J. E. Gschwend, T. Seufferlein, T. Gress, G. Adler, M. G. Bachem, *J. Cell Sci.* **2007**, *120*, 512.
[105] M. Määttä, Y. Soini, A. Liakka, H. Autio-Harmainen, *Clin. Cancer Res.* **2000**, *6*, 2726.
[106] K. Koikawa, K. Ohuchida, Y. Ando, S. Kibe, H. Nakayama, S. Takesue, S. Endo, T. Abe, T. Okumura, C. Iwamoto, T. Moriyama, K. Nakata, Y. Miyasaka, T. Ohtsuka, E. Nagai, K. Mizumoto, M. Hashizume, M. Nakamura, *Cancer Lett.* **2018**, *425*, 65.

[107] Z. Wang, Y. Li, D. Kong, S. Banerjee, A. Ahmad, A. S. Azmi, S. Ali, J. L. Abbruzzese, G. E. Gallick, F. H. Sarkar, *Cancer Res.* **2009**, *69*, 2400.
[108] H.-Q. Ju, H. Li, T. Tian, Y.-X. Lu, L. Bai, L.-Z. Chen, H. Sheng, H.-Y. Mo, J.-B. Zeng, W. Deng, P. J. Chiao, R.-H. Xu, *J. Pineal Res.* **2016**, *60*, 27.
[109] M. V. Apte, J. S. Wilson, A. Lugea, S. J. Pandol, *Gastroenterology* **2013**, *144*, 1210.
[110] J. Tao, G. Yang, W. Zhou, J. Qiu, G. Chen, W. Luo, F. Zhao, L. You, L. Zheng, T. Zhang, Y. Zhao, *J. Hematol. Oncol.* **2021**, *14*, 14.
[111] P. Büchler, H. A. Reber, M. Büchler, S. Shrinkante, M. W. Büchler, H. Friess, G. L. Semenza, O. J. Hines, *Pancreas* **2003**, *26*, 56.
[112] E. Hessmann, M. S. Patzak, L. Klein, N. Chen, V. Kari, I. Ramu, T. E. Bapiro, K. K. Frese, A. Gopinathan, F. M. Richards, D. I. Jodrell, C. Verbeke, X. Li, R. Heuchel, J. M. Löhr, S. A. Johnsen, T. M. Gress, V. Ellenrieder, A. Neesse, *Gut* **2018**, *67*, 497.
[113] M. Amrutkar, I. P. Gladhaug, *Cancers* **2017**, *9*, 157.
[114] S. Khan, M. C. Ebeling, N. Chauhan, P. A. Thompson, R. K. Gara, A. Ganju, M. M. Yallapu, S. W. Behrman, H. Zhao, N. Zafar, M. M. Singh, M. Jaggi, S. C. Chauhan, *Cancer Res.* **2015**, *75*, 2292.
[115] M. Schober, R. Jesenofsky, R. Faissner, C. Weidenauer, W. Hagmann, P. Michl, R. Heuchel, S. Haas, J.-M. Löhr, *Cancers* **2014**, *6*, 2137.
[116] W. Xiao, M. Pahlavanneshan, C.-Y. Eun, X. Zhang, C. DeKalb, B. Mahgoub, H. Knaneh-Monem, S. Shah, A. Sohrabi, S. K. Seidlits, R. Hill, *Matrix Biol. Plus* **2022**, *14*, 100111.
[117] Z. Gu, Y. Du, X. Zhao, C. Wang, *Cancer Lett.* **2021**, *521*, 98.
[118] C. J. Whatcott, R. G. Posner, D. D. Von Hoff, H. Han, in *Pancreatic Cancer and Tumor Microenvironment* (Eds: P. J. Grippo, H. G. Munshi), Transworld Research Network, Trivandrum **2012**, Ch. 8.
[119] M. A. Shields, S. Dangi-Garimella, A. J. Redig, H. G. Munshi, *Biochem. J.* **2012**, *441*, 541.
[120] N. Awasthi, A. J. Mikels-Vigdal, E. Stefanutti, M. A. Schwarz, S. Monahan, V. Smith, R. E. Schwarz, *J. Cell. Mol. Med.* **2019**, *23*, 3878.
[121] A. Gregori, C. Bergonzini, M. Capula, G. Mantini, F. Khojasteh-Leylakoohi, A. Comandatore, G. Khalili-Tanha, A. Khooei, L. Morelli, A. Avan, E. H. Danen, T. Schmidt, E. Giovannetti, *Cancers* **2023**, *15*, 628.
[122] S. K. Shukla, V. Purohit, K. Mehla, V. Gunda, N. V. Chaika, E. Vernucci, R. J. King, J. Abrego, G. D. Goode, A. Dasgupta, A. L. Illies, T. Gebregiworgis, B. Dai, J. J. Augustine, D. Murthy, K. S. Attri, O. Mashadova, P. M. Grandgenett, R. Powers, Q. P. Ly, A. J. Lazenby, J. L. Grem, F. Yu, J. M. Matés, J. M. Asara, J.-W. Kim, J. H. Hankins, C. Weekes, M. A. Hollingsworth, N. J. Serkova, et al., *Cancer Cell* **2017**, *32*, 71.e77.

